PHYSICAL REVIEW D **92,** 114029 (2015)

Spectrum of heavy baryons in the quark model

T. Yoshida,[1,*] E. Hiyama,[2,1,3] A. Hosaka,[4,3] M. Oka,[1,3] and K. Sadato[4,†]

[1]*Department of Physics, Tokyo Institute of Technology, Meguro 152-8551, Japan*
[2]*Nishina Center for Accelerator-Based Science, RIKEN, Wako 351-0198, Japan*
[3]*Advanced Science Research Center, Japan Atomic Energy Agency, Tokai, Ibaraki 319-1195, Japan*
[4]*Research Center for Nuclear Physics (RCNP), Osaka University, Ibaraki, Osaka 567-0047, Japan*

(Received 6 October 2015; published 28 December 2015)

Single- and double-heavy baryons are studied in the constituent quark model. The model Hamiltonian is chosen as a standard one with two exceptions: (1) the color-Coulomb term depends on quark masses and (2) an antisymmetric LS (spin-orbit) force is introduced. Model parameters are fixed by the strange baryon spectra, Λ and Σ baryons. The masses of the observed charmed and bottomed baryons are, then, fairly well reproduced. Our focus is on the low-lying negative-parity states, in which the heavy baryons show specific excitation modes reflecting the mass differences of heavy and light quarks. By changing quark masses from the SU(3) limit to the strange quark mass, and, further, to the charm and bottom quark masses, we demonstrate that the spectra change from the SU(3) symmetry patterns to the heavy-quark-symmetry ones.

DOI: 10.1103/PhysRevD.92.114029 PACS numbers: 12.39.Jh, 14.20.Lq, 14.20.Mr

I. INTRODUCTION

Recent hadron physics has been stimulated by observations of exotic hadrons with heavy quarks. So-called X, Y, and Z mesons most likely contain a hidden heavy quark and antiquark pair, either $\bar{c}c$ or $\bar{b}b$. In addition, they may contain a light quark and antiquark pair, thus forming a multiquark configuration near the threshold region of open flavor. For instance, $X(3872), Z_b(10610, 10850)$ are expected to be hadronic molecules of $D\bar{D}^*$, $B\bar{B}^*$, or $B^*\bar{B}^*$ via the strong correlation of a quark and antiquark pair [1,2]. Furthermore, the pentaquarks $P_c(4380)$ and $P_c(4450)$ recently discovered by LHCb [3] may also have such a structure.

Theoretically, diquark qq correlations may also play an important role, leading to the idea of compact tetraquarks [4,5]. In fact, the diquark correlations have been considered for long time in many different contexts [6] to explain the mass ordering of light scalar mesons, weak decays of hyperons, missing nucleon resonances, the novel phase structure of the quark matter, and so on. In QCD, the correlation densities of the two light quarks were measured, having indicated a strong attraction in a so-called good diquark pair [7]. In reality, the evidence should be also seen in masses of excited states. Charmed baryons with two light quarks may provide a good opportunity for such a study.

Pioneering work was done some time ago by Copley *et al.* [8] in a constituent quark model, which was later elaborated by Roberts and Pervin [9]. They studied various excited states of charmed and bottomed baryons by solving three-quark systems explicitly. A motivation of the present work is to further point out the behavior of various properties of heavy baryons as functions of the heavy-quark mass, smoothly interpolating the SU(3) limit of equal quark masses and the heavy-quark limit. Such a study in different flavor regions is useful to systematically understand the nature of spectrum, in particular the roles of the two internal motions when baryons are regarded as three-body systems of quarks. The structure information, then, must show up sensitively in various transition amplitudes of decays and productions, which can be studied experimentally as planned at J-PARC and FAIR.

Let us start by briefly showing the essential features of the three-quark systems, with one heavy quark (Q) of mass m_Q and the two light quarks (q) of equal mass m_q, using a nonrelativistic quark model with a harmonic oscillator potential for confinement [8].

It is convenient to introduce the Jacobi coordinates $\boldsymbol{\lambda} = \boldsymbol{r}_Q - \frac{\boldsymbol{r}_{q1}+\boldsymbol{r}_{q2}}{2}$ and $\boldsymbol{\rho} = \boldsymbol{r}_{q2} - \boldsymbol{r}_{q1}$, with obvious notations. In the harmonic oscillator potential, the two degrees of freedom decouple and the Hamiltonian can be written simply as a sum of the two parts,

$$H = \sum_i \frac{\boldsymbol{p}_i^2}{2m_i} + \sum_{i<j} \frac{k}{2}|\boldsymbol{r}_i - \boldsymbol{r}_j|^2 = \frac{\boldsymbol{p}_\rho^2}{2m_\rho} + \frac{\boldsymbol{p}_\lambda^2}{2m_\lambda} + \frac{m_\rho \omega_\rho{}^2}{2}\boldsymbol{\rho}^2 + \frac{m_\lambda \omega_\lambda{}^2}{2}\boldsymbol{\lambda}^2, \quad (1)$$

where m_ρ and m_λ denote the reduced masses

$$m_\rho = \frac{m_q}{2}, \qquad m_\lambda = \frac{2m_q m_Q}{2m_q + m_Q} \quad (2)$$

and the oscillator frequencies ω_ρ and ω_λ are given by

*t.yoshida@th.phys.titech.ac.jp
†Present address: G-search Ltd., Tamachi 108-0022, Japan.

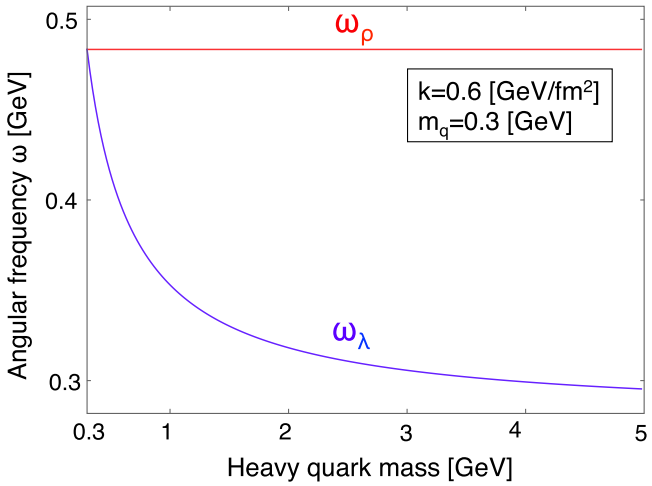

FIG. 1 (color online). Heavy-quark mass dependence of excited energies of the λ mode (red solid line) and the ρ mode (blue solid line) in Eq. (1).

$$\omega_\rho = \sqrt{\frac{3k}{2m_\rho}}, \qquad \omega_\lambda = \sqrt{\frac{2k}{m_\lambda}}. \tag{3}$$

The ratio of the two excited energies is then given by

$$\frac{\omega_\lambda}{\omega_\rho} = \sqrt{\frac{1}{3}(1 + 2m_q/m_Q)} \leq 1. \tag{4}$$

In the SU(3) limit, when the quark masses are equal, $m_q = m_Q$, the λ and ρ modes degenerate, $\omega_\lambda = \omega_\rho$. However, when $m_Q > m_q$, the excited energy of the λ mode is smaller than that of the ρ mode, $\omega_\lambda < \omega_\rho$ (see Fig. 1). Thus, we expect that in the heavy-quark sector, the λ excitation modes become dominant for low-lying states of singly heavy-quark baryons. In contrast, when $m_Q < m_q$, which corresponds to doubly heavy-quark baryons, we have $\omega_\lambda > \omega_\rho$; therefore, the ρ excitation modes become dominant. It is shown that this feature is rather general for nonrelativistic potential models except for the case when the Coulomb type potential of $1/r$ dominates the binding.

One important symmetry structure realized in the heavy-quark hadrons is the heavy-quark spin symmetry (HQS) [10]. In the heavy-quark limit, the interactions which depend on the spin of the heavy quark disappear. Thus, in a single-heavy hadron the heavy-quark spin $\boldsymbol{s}_Q$ is conserved (i.e., $[H, \boldsymbol{s}_Q] = 0$); with the conservation of the total angular momentum $\boldsymbol{J}$, one sees that $\boldsymbol{j} \equiv \boldsymbol{J} - \boldsymbol{s}_Q$ which is the angular momentum carried by the light quarks (including all the orbital angular momenta) is also conserved. We will call j the light-spin component. Consequently, the two states whose quantum numbers are $J = j + 1/2$ and $J = j - 1/2$ will be degenerate. They form a heavy-quark spin doublet, except for $j = 0$, which yields a HQS singlet. A simple example of a HQS doublet is the pair of $\Sigma_Q(1/2^+)$ and $\Sigma_Q(3/2^+)$. The mass differences $\Sigma_s(3/2^+) - \Sigma_s(1/2^+) = 174$ MeV, $\Sigma_c(3/2^+) - \Sigma_c(1/2^+) = 63$ MeV and $\Sigma_b(3/2^+) - \Sigma_b(1/2^+) = 22$ MeV decrease as m_Q becomes large.

We organize this paper as follows. In Sec. II, we present our formulation of the nonrelativistic constituent quark model. The Hamiltonian and the quark interaction are introduced in Sec. II A; we employ a linear potential for quark confinement supplemented by spin-spin, tensor, and spin-orbit (LS) forces. The antisymmetric LS force is also needed to guarantee the heavy-quark symmetry. In Sec. II B, the Gaussian expansion method is introduced to solve the three-quark system. When the heavy-quark mass is varied from $m_Q = m_q$ to $m_Q \to \infty$, the symmetry of the spectrum then changes from the SU(3) to the heavy-quark spin symmetry. In Sec. II C, the relation of the two symmetry limits and mixings of the two internal excitation modes are discussed. The results of the present work are presented in Sec. III. The results of single-heavy baryons and those of double-heavy baryons are discussed in Secs. III A and III B, respectively. The properties of the λ and ρ modes are discussed in detail in Sec. III C. In Sec. III D, the heavy-quark limit is investigated. Finally, a summary is given in Sec. IV.

II. FORMALISM

A. Hamiltonian

In this subsection, we discuss our model Hamiltonian in detail. In the nonrelativistic quark model, baryons are formed by three valence (constituent) quarks. They are confined by a confining potential and interact with each other by residual two-body interactions. Their internal motions are then described by the two spatial variables $\boldsymbol{\rho}$ and $\boldsymbol{\lambda}$. In other models of baryons, nonquark degrees of freedom are considered such as constituent gluons and confining fields. Their signals in baryon excitations are, however, not yet confirmed in experiments, and are expected to lie at higher energies than the low-lying quark excitation modes. Empirically these justify the applicability of the quark model, especially for low-lying excitation modes.

Thus our Hamiltonian is written as

$$H = K + V_{\text{con}} + V_{\text{short}}, \tag{5}$$

where the kinetic energy, K, the confinement potential, V_{con}, and the short-range interaction, V_{short}, are given as

$$K = \sum_i \left(m_i + \frac{\boldsymbol{p}^2{}_i}{2m_i} \right) - K_G, \tag{6}$$

$$V_{\text{con}} = \sum_{i<j} \frac{b r_{ij}}{2} + C, \tag{7}$$

$$V_{\rm short} = \sum_{i<j}\Bigg[-\frac{2\alpha^{\rm Coul}}{3r_{ij}} + \frac{16\pi\alpha^{\rm ss}}{9m_i m_j}\boldsymbol{s}_i\cdot\boldsymbol{s}_j\frac{\Lambda^2}{4\pi r_{ij}}\exp(-\Lambda r_{ij}) + \frac{\alpha^{\rm so}(1-\exp(-\Lambda r_{ij}))^2}{3{r_{ij}}^3} \times\Bigg[\left(\frac{1}{m_i^2}+\frac{1}{m_j^2}+4\frac{1}{m_i m_j}\right)\boldsymbol{L}_{ij}\cdot(\boldsymbol{s}_i+\boldsymbol{s}_j) + \left(\frac{1}{m_i^2}-\frac{1}{m_j^2}\right)\boldsymbol{L}_{ij}\cdot(\boldsymbol{s}_i-\boldsymbol{s}_j)\Bigg] + \frac{2\alpha^{\rm ten}(1-\exp(-\Lambda r_{ij}))^2}{3m_i m_j {r_{ij}}^3}\left(\frac{3(\boldsymbol{s}_i\cdot\boldsymbol{r_{ij}})(\boldsymbol{s}_j\cdot\boldsymbol{r_{ij}})}{{r_{ij}}^2}-\boldsymbol{s}_i\cdot\boldsymbol{s}_j\right)\Bigg]. \quad (8)$$

In Eq. (6), m_i is the constituent quark mass of the ith quark, and the center-of-mass energy, K_G, is subtracted so that the kinetic energy consists only those for the ρ and λ coordinates. In Eq. (7), we employ the linear confinement potential with the b parameter corresponding to the string tension and $\boldsymbol{r}_{ij}=\boldsymbol{r}_i-\boldsymbol{r}_j$ is the relative coordinate. In Eq. (8), $\boldsymbol{L}_{ij}=(\boldsymbol{r}_i-\boldsymbol{r}_j)\times(m_j\boldsymbol{p}_i-m_i\boldsymbol{p}_j)/(m_i+m_j)$ is the relative orbital angular momentum and $\boldsymbol{s}_i(=\sigma_i/2)$ is the spin operator of the ith quark. The components of Eq. (8) are inferred by the one-gluon exchange (OGE), which requires only one coupling constant common to the four terms. Practically, however, they may have different origins other than the OGE; therefore, we treat the four coupling strengths, $\alpha^{\rm Coul}$, $\alpha^{\rm ss}$, $\alpha^{\rm so}$, and $\alpha^{\rm ten}$ as independent parameters for better description of baryon masses.

The third term in Eq. (8) consists of the symmetric LS (SLS) potential, $V_{\rm SLS}$, with $\boldsymbol{L}_{ij}\cdot(\boldsymbol{s}_i+\boldsymbol{s}_j)$ and the antisymmetric LS (ALS) potential, $V_{\rm ALS}$, with $\boldsymbol{L}_{ij}\cdot(\boldsymbol{s}_i-\boldsymbol{s}_j)$. The ALS is necessary to guarantee the heavy quark symmetry. The terms dependent on the heavy-quark spin $\boldsymbol{s_Q}$ of the $V_{\rm SLS}$ and $V_{\rm ALS}$ in a single-heavy baryon are given by

$$V_{\rm SLS}\to\sum_{i=1,2}\frac{\alpha^{\rm so}(1-\exp(-\Lambda r_{iQ}))^2}{3r_{iQ}^3} \times\left(\frac{1}{m_i^2}+\frac{1}{m_Q^2}+\frac{4}{m_i m_Q}\right)\boldsymbol{L}_{iQ}\cdot\boldsymbol{s}_Q, \quad (9)$$

$$V_{\rm ALS}\to\sum_{i=1,2}\frac{\alpha^{\rm so}(1-\exp(-\Lambda r_{iQ}))^2}{3r_{iQ}^3} \quad (10)$$

$$\times\left(\frac{1}{m_i^2}-\frac{1}{m_Q^2}\right)\boldsymbol{L}_{iQ}\cdot(-\boldsymbol{s}_Q), \quad (11)$$

where we choose $i=3$ for the heavy quark. Then, by summing the parts from the SLS and ALS, the $\boldsymbol{L_Q}\cdot\boldsymbol{s_Q}$ is always proportional to $1/m_Q$ or higher. Thus the $\boldsymbol{s}_Q$ dependence disappears in the $m_Q\to\infty$ limit, and the heavy-quark symmetry is guaranteed.

Recently, it was suggested by a Lattice QCD calculation [11] that the strength, $\alpha^{\rm Coul}$, of the color Coulomb force depends significantly on the quark mass. In our study, we therefore assume that $\alpha^{\rm Coul}$ for the $i-j$ pair of quarks depends on the reduced mass, $\mu_{ij}=\frac{m_i m_j}{m_i+m_j}$, as follows:

$$\alpha^{\rm Coul}=\frac{K}{\mu_{ij}}. \quad (12)$$

We summarize 10 parameters in the Hamiltonian employed here in Table I. The parameters are determined from experimental data of the strange baryon spectrum (see Table II). First, we switch off the LS and tensor force to determine the parameters C, $\alpha_{\rm ss}$, m_q, m_s, Λ, and K from the positive parity state. Then, we determine $\alpha^{\rm so}$ and b from negative parity states. The details of how to determine the parameters are as follows:

(i) The constant term C: In the constituent quark models, we can predict mass differences between different states, but the absolute values can not be determined. In our work, we introduce the constant C to reproduce the ground state of $\Lambda(1115)$ and we assume that the constant C is independent of the constituent quark mass; namely, we use the same value for the charmed baryons.

(ii) Spin-spin term: The spin-spin term in the Hamiltonian is responsible for the splitting among Λ, Σ, and Σ^*. This term depends on $\alpha^{\rm ss}$, m_q, m_s, and Λ. Because we have four parameters for three states to be fitted, we fix $m_q=300$ MeV, which is the standard value suggested from the magnetic moment of the baryon in the constituent quark model, and then we determine the other parameters to reproduce the masses of Λ, Σ, Σ^*.

TABLE I. Parameters in the Hamiltonian. We determine m_q, m_s, b, K, α^{ss}, and Λ to reproduce strange baryons, and m_c and m_b are determined from the ground state of Λ_c and Λ_b.

m_q (MeV)	m_s (MeV)	m_c (MeV)	m_b (MeV)	b (GeV^2)	K (MeV)	$\alpha^{\rm ss}$	$\alpha^{\rm so}$ $(=\alpha^{\rm ten})$	C (MeV)	Λ (fm^{-1})
300	510	1750	5112	0.165	90	1.2	0.077	−1139	3.5

TABLE II. Calculated energy spectra and corresponding experimental data of Λ_s, Σ_s, and Ξ_{ss}. We take the three-star and four-star resonances in PDG except for the first $1/2^-$ state of Σ_s, which has only two stars.

Λ_s		
J^P	Theory (MeV)	Experiment (MeV)
$\frac{1}{2}^+$	1116	1116
	1799	1560–1700
	1922	1750–1850
$\frac{3}{2}^+$	1882	1850–1910
	2030	
	2100	
$\frac{5}{2}^+$	1891	1815–1825
	2045	2090–2140
	2143	
$\frac{1}{2}^-$	1526	1405
	1665	1660–1680
	1777	1720–1850
$\frac{3}{2}^-$	1537	1520
	1685	1685–1695
	1810	
$\frac{5}{2}^-$	1814	1810–1830
	2394	
	2448	

Σ_s		
J^P	Theory (MeV)	Experiment (MeV)
$\frac{1}{2}^+$	1197	1192
	1895	1630–1690
	2016	
$\frac{3}{2}^+$	1391	1385
	2004	
	2028	
$\frac{5}{2}^+$	2012	1900–1935
	2085	
	2091	
$\frac{1}{2}^-$	1654	(≈1620)
	1734	1730–1800
	1751	
$\frac{3}{2}^-$	1660	1665–1685
	1755	1900–1950
	1760	
$\frac{5}{2}^-$	1762	1770–1780
	2324	
	2427	

Ξ_{ss}		
J^P	Theory (MeV)	Experiment (MeV)
$\frac{1}{2}^+$	1325	1314
	1962	
	2131	

(Table continued)

TABLE II. (*Continued*)

Ξ_{ss}		
J^P	Theory (MeV)	Experiment (MeV)
$\frac{3}{2}^+$	1525	1530
	2034	
	2115	
$\frac{5}{2}^+$	2040	
	2166	
	2211	
$\frac{1}{2}^-$	1778	
	1875	
	1910	
$\frac{3}{2}^-$	1782	1820
	1877	
	1920	
$\frac{5}{2}^-$	1933	
	2460	
	2518	

(iii) The parameter K: In our calculation, we introduce α^{Coul} as a quark-mass-dependent form as given by Eq. (12). Thus, the Coulomb force can contribute to the mass splitting between the ground states of $\Lambda_s(\Sigma_s)$, Ξ_{ss}, and Ω_{sss}. This force also contributes to the mass differences between the ground state and the excited states. We determine the parameter K to reproduce $\Xi(1/2^+)$ and the mass difference between the ground state and the excited states.

(iv) The linear confinement b: Our emphasis in the present study is on the P-wave states. The parameters which mainly determine the mass differences are b and K. K is determined from $\Xi(1/2^+)$ as mentioned above and we determine the parameter b to reproduce the splitting between the ground state and the P-wave state.

(v) The spin-orbit coupling α^{so}: The strength α^{so} of the spin-orbit force may be determined by the splitting of the P-wave baryons, such as $\Lambda(1/2^-)$ and $\Lambda(3/2^-)$. However, we do not use the lowest $\Lambda(1/2^-)$, $= \Lambda(1405)$, because various recent studies on the $\Lambda(1405)$ resonance suggests that this is not simply a pure three-quark state, but rather a $N\bar{K}$ molecularlike state. Therefore, we determine the parameter α^{so} to reproduce the splitting between the second $\Lambda(1/2^-)$ and $\Lambda(3/2^-)$, namely $\Lambda(1670)$ and $\Lambda(1690)$. Thus, as expected, α_{so} becomes very small, much smaller than α_{ss}. If the spin-spin and LS forces come only from the OGE, then their values are not consistent. However, other sources of quark interactions, including the relativistic correlations to the confinement and instanton-induced interaction (III), may also contribute the LS interaction. It was pointed out [12] that the LS

forces from OGE and III are opposite. Then, the discrepancy between α^{ss} and α^{so} can be explained.

(vi) The strength α^{ten}: The tensor force in the Hamiltonian contributes mainly to the positive parity $\Sigma(1/2^+)$, $\Sigma(3/2^+)$ and the lowest negative states. It has been known that the tensor force is weak and does not contribute much except for generating mixings of $S = 1/2$ and $3/2$ states. We choose α^{ten} equal to α^{so}.

(vii) Charm- and bottom-quark mass, m_c, m_b: We fit the charm-quark mass m_c (bottom-quark mass m_b) to the ground state of Λ_c (Λ_b). These values contribute to the mass splittings as well as the absolute values, but once we determine the other parameters in the strange sector, m_c and m_b are determined uniquely.

From Table II, we find that our results reproduce most of the known strange baryon masses, except for the second $J^P = 1/2^+$ state and the first $J^P = 1/2^-$ state. It is well known that the Roper resonance $N(1440)$, the second $J^P = 1/2^+$ state, is lighter than lowest $J^P = 1/2^-$ state, which is incompatible with the quark model predictions. Similarly, in the strange sector, the Roper-like states $\Lambda(1600)$ and $\Sigma(1660)$ are predicted at higher masses than experiment. The origin of these discrepancies may reside outside the simple three-quark picture of the baryons in the quark model. We therefore omit these states from the fitting in the present analysis.

B. Baryon wave function

We here consider three-quark systems (Table III) with one heavy quark, $Q = (c \text{ or } b)$, and with two or three heavy quarks with the same flavor, i.e., $QQ = (cc \text{ or } bb)$ and $QQQ = (ccc \text{ or } bbb)$. The remaining quarks are u, d, or s. We classify the baryons according to the number of heavy quarks, the strangeness, $\mathcal{S}$, and the total isospin, T. The last column of Table III shows the isospin wave function where $\eta_0 = 1$.

TABLE III. Heavy baryons and their flavor contents. We use the isopin classification so that q stands collectively for the u and d quarks. Q denotes a c or b quark. We do not consider mixing of c and b.

Heavy baryons	Isospin $\mathcal{S}$	Strangeness T	Isospin wave function
$\Lambda_Q = [qq]_{T=0}Q$	0	0	$[[\eta_{1/2}\eta_{1/2}]_{t=0}\eta_0]_{T=0}$
$\Sigma_Q = [qq]_{T=1}Q$	0	1	$[[\eta_{1/2}\eta_{1/2}]_{t=1}\eta_{1/2}]_{T=1}$
$\Xi_Q = sqQ$	−1	1/2	$[[\eta_0\eta_{1/2}]_{t=1/2}\eta_0]_{T=1/2}$
$\Omega_Q = ssQ$	−2	0	1
$\Xi_{QQ} = QQq$	0	1/2	$[[\eta_0\eta_0]_{t=0}\eta_{1/2}]_{T=1/2}$
$\Omega_{QQ} = QQs$	−1	0	1
$\Omega_{QQQ} = QQQ$	0	0	1

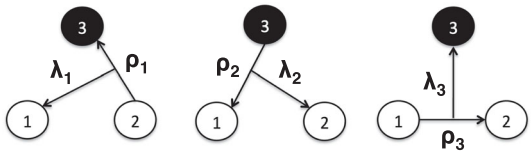

FIG. 2. Jacobi coordinates for the three-body system. We place the heavy quark as the third particle in the case of single-heavy baryons, while the first and second particles are heavy quarks in double-heavy baryons.

In expressing three-quark wave functions, we introduce three sets of Jacobi coordinates, which we call channels (Fig. 2). The Jacobi coordinates in each channel c ($c = 1$, 2, 3) are defined as

$$\boldsymbol{\lambda}_c = \boldsymbol{r}_k - \frac{m_i \boldsymbol{r}_i + m_j \boldsymbol{r}_j}{m_i + m_j}, \tag{13}$$

$$\boldsymbol{\rho}_c = \boldsymbol{r}_j - \boldsymbol{r}_i, \tag{14}$$

where (i, j, k) are given by Table IV.

The total wave function is given as a superposition of the channel wave functions as

$$\Phi^{JM}_{\text{total}} = \sum_{c\alpha} C_{c,\alpha} \Phi^{(c)}_{JM,\alpha}(\boldsymbol{\rho}_c, \boldsymbol{\lambda}_c), \tag{15}$$

where the index α represents $\{s, S, \ell, L, I, n, N\}$. Here s is the spin of the (i, j) quark pair, S is the total spin, ℓ and L are the orbital angular momentum for the coordinate ρ and λ, respectively, and I is the total orbital angular momentum. The coupling scheme of the spin and angular momenta is as

$$\begin{aligned} \boldsymbol{s} &= \boldsymbol{s}_i + \boldsymbol{s}_j; \qquad \boldsymbol{s} + \boldsymbol{s}_k = \boldsymbol{S}; \\ \boldsymbol{\ell} + \boldsymbol{L} &= \boldsymbol{I}; \qquad \boldsymbol{S} + \boldsymbol{I} = \boldsymbol{J}. \end{aligned} \tag{16}$$

The wave function for channel c is given by

$$\Phi^{(c)}_{JM}(\boldsymbol{\rho}_c, \boldsymbol{\lambda}_c) = \phi_c \otimes [X^{(c)}_{S,s} \otimes \Phi^{(c)}_{\ell,L,I}]_{JM} \otimes H^{(c)}_{T,t}, \tag{17}$$

where the color wave function, ϕ_c, the spin wave function, X_S, the orbital wave function, Φ_I, and the isospin wave function, H_T, are given by

$$\phi_c = \frac{1}{\sqrt{6}}(rgb - rbg + gbr - grb + brg - bgr), \tag{18}$$

TABLE IV. The quark assignments (i, j, k) for the Jacobi channels.

Channel	i	j	k
1	2	3	1
2	3	1	2
3	1	2	3

$$X^{(c)}_{S,s} = [[\chi_{1/2}(i)\chi_{1/2}(j)]_s \chi_{1/2}(k)]_S, \tag{19}$$

$$H^{(c)}_{T,t} = [[\eta_{\tau_i}(i)\eta_{\tau_j}(j)]_t \eta_{\tau_k}(k)]_T, \tag{20}$$

$$\Phi^{(c)}_{\ell,L,I} = [\phi^{(c)}_\ell(\boldsymbol{\rho}_c)\phi^{(c)}_L(\boldsymbol{\lambda}_c)]_I, \tag{21}$$

$$\phi^{(c)}_\ell(\boldsymbol{\rho}_c) = N_{n\ell}\rho_c^\ell e^{-\beta_n\rho_c^2} Y_{\ell m}(\hat{\boldsymbol{\rho}}_c), \tag{22}$$

$$\phi^{(c)}_L(\boldsymbol{\lambda}_c) = N_{NL}\lambda_c^L e^{-\gamma_N\lambda_c^2} Y_{LM}(\hat{\boldsymbol{\lambda}}_c). \tag{23}$$

In Eq. (18), r, g, b denote the color of the quark, and the color-singlet wave function is totally antisymmetric. In Eq. (19), $\chi_{1/2}$ is the spin wave function of the quark, while η_τ in Eq. (20) is the isospin wave function with τ defined by

$$\tau = \begin{cases} 1/2 & \text{for } u, d \\ 0 & \text{for } s, c, b. \end{cases} \tag{24}$$

We consider the quark antisymmetrization for the light quarks, u and d, and the heavy quarks, s, c, b, separately. Then, for single-heavy baryons, antisymmetrization is applied only to the light quarks. As the color wave function is always totally antisymmetric, the spin, isospin and the orbital angular momentum in the channel $c = 3$ should satisfy

$$\ell + s + t = \text{even} \quad \text{for } \Lambda_Q, \Sigma_Q, \tag{25}$$

where ℓ, s, t are the orbital angular momentum, total spin, and isospin of the two light quarks. Similarly, the heavy quarks are antisymmetrized in the double-heavy baryons as

$$\ell + s + 1 = \text{even} \quad \text{for } \Xi_{QQ}, \Omega_Q, \Omega_{QQ}, \tag{26}$$

where ℓ, s, t are the corresponding ones for the heavy quarks. Considering the antisymmetrization and the combinations of the angular momenta, we obtain possible assignments of the angular momenta for the low-lying $\Lambda_Q(1/2^+)$ in Table V, where we take all the combinations satisfying $\ell + L \leq 2$.

In solving the Schrödinger equation, we use the Gaussian expansion method [13], where the orbital wave functions are expanded, in Eqs. (22) and (23), by Gaussian functions with the range parameters, β_n and γ_N, chosen as

$$\beta_n = 1/r_n^2, \qquad r_n = r_1 a^{n-1} (n = 1, \ldots, n_{\max}), \tag{27}$$

$$\gamma_N = 1/R_N^2, \qquad R_N = R_1 b^{N-1} (N = 1, \ldots, N_{\max}). \tag{28}$$

In Eqs. (22) and (23), $N_{n\ell}(N_{NL})$ denotes the normalization constant of the Gaussian basis. The coefficients $C_{c,\alpha}$ of the variational wave function, Eq. (15), are determined by the Rayleigh-Ritz variational principle. In order to check that the energy converges to the required precision, we change the number of bases and plot the eigenenergy of the lowest-lying $\Lambda_c(3/2^-)$ in Fig. 3. The filled points are the results from the calculation only using the channel $c = 3$, while the open circles are the results from the three-channel calculation (Fig. 2). One sees that when we take only one channel, the convergence is slow and has not yet reached the required precision at $N_{\max} = n_{\max} = 10$.

TABLE V. Combinations of the spin and orbital angular momenta in channel 3 of the low-lying $\Lambda(1/2^+)$. In our study, we restrict the total angular momentum up to 2, $\ell + L = 0, 2$.

Channel	ℓ	L	I	s	S
3	0	0	0	0	1/2
3	1	1	0	1	1/2
3	1	1	1	1	1/2
3	1	1	1	1	3/2
3	1	1	2	1	3/2

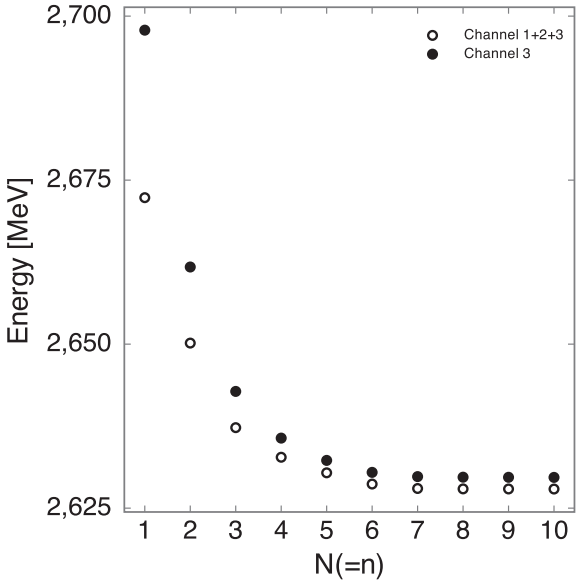

FIG. 3. Convergence of the energy of the lowest $\Lambda_c(3/2^-)$ for increasing the number of bases functions.

C. Heavy-quark limit

One of the aims of this paper is to see how the heavy-baryon spectrum changes when the heavy-quark mass m_Q changes. Two limits are important: the SU(3) limit with $m_Q = m_q$, and the HQ limit, $m_Q \to \infty$.

In the limit $m_Q \to m_q$, the spectrum is classified by the SU(3) representations. For instance, the lowest P-wave baryons are expected to belong to the SU(6) 70-dimensional representation, which contains $^2\mathbf{1}$, $^2\mathbf{8}$, $^4\mathbf{8}$, and $^2\mathbf{10}$. Here the upper index number is the spin multiplicity and the bold number represents the SU(3) multiplicity. On the other hand, in the HQ limit, $m_Q \to \infty$,

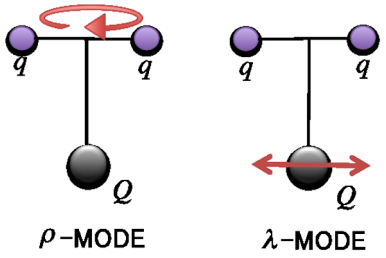

FIG. 4 (color online). The ρ- and λ-mode excitations of the single-heavy baryon.

as we have discussed in Sec. I, the P-wave baryons are better classified by the ρ- and λ-mode excitations (Fig. 4). Here we derive relations between the two pictures.

Let us consider single-heavy Λ_Q and Σ_Q baryons. We put the heavy quark Q as the third quark. Then the orbital-spin wave functions of Λ_Q and Σ_Q in the SU(3) limit are given by

$$\Psi(\Lambda_Q;{}^2\mathbf{1}) = \frac{1}{\sqrt{2}}(X_{1/2,1}\Phi_{1,0,1} - X_{1/2,0}\Phi_{1,1,0}), \quad (29)$$

$$\Psi(\Lambda_Q;{}^2\mathbf{8}) = \frac{1}{\sqrt{2}}(X_{1/2,1}\Phi_{1,0,1} + X_{1/2,0}\Phi_{1,1,0}), \quad (30)$$

$$\Psi(\Lambda_Q;{}^4\mathbf{8}) = X_{3/2,1}\Phi_{1,0,1} \quad (31)$$

and

$$\Psi(\Sigma_Q;{}^2\mathbf{10}) = \frac{1}{\sqrt{2}}(X_{1/2,1}\Phi_{1,1,0} + X_{1/2,0}\Phi_{1,0,1}), \quad (32)$$

$$\Psi(\Sigma_Q;{}^2\mathbf{8}) = \frac{1}{\sqrt{2}}(X_{1/2,1}\Phi_{1,1,0} - X_{1/2,0}\Phi_{1,0,1}), \quad (33)$$

$$\Psi(\Sigma_Q;{}^4\mathbf{8}) = X_{3/2,1}\Phi_{1,1,0}. \quad (34)$$

In the SU(3) limit, the ${}^2\mathbf{8}(S=1/2)$ and ${}^4\mathbf{8}(S=3/2)$ can be mixed with the spin-spin/spin-orbit forces [if we further argue SU(6), they do not mix]. For $m_q < m_Q$, $\Psi(\Lambda_Q;{}^2\mathbf{1})$ and $\Psi(\Lambda_Q;{}^2\mathbf{8})$ may mix with each other; in the large m_Q limit, they are reduced to the λ-mode, $\Phi_{1,1,0}$, and the ρ-mode, $\Phi_{1,0,1}$, excitations. Representing the $\lambda(\rho)$ mode with the total spin S by ${}^{2S+1}\lambda({}^{2S+1}\rho)$, we obtain

$$\Psi(\Lambda_Q;{}^2\lambda) = X_{1/2,0}\Phi_{1,1,0} = \frac{1}{\sqrt{2}}(\Psi(\Lambda_Q;{}^2\mathbf{8}) - \Psi(\Lambda_Q;{}^2\mathbf{1})), \quad (35)$$

$$\Psi(\Lambda_Q;{}^2\rho) = X_{1/2,1}\Phi_{1,0,1} = \frac{1}{\sqrt{2}}(\Psi(\Lambda_Q;{}^2\mathbf{8}) + \Psi(\Lambda_Q;{}^2\mathbf{1})), \quad (36)$$

$$\Psi(\Lambda_Q;{}^4\rho) = X_{3/2,1}\Phi_{1,0,1} = \Psi(\Lambda_Q;{}^4\mathbf{8}) \quad (37)$$

for the Λ_Q baryons and

$$\Psi(\Sigma_Q;{}^2\lambda) = X_{1/2,1}\Phi_{1,1,0} = \frac{1}{\sqrt{2}}(\Psi(\Sigma_Q;{}^2\mathbf{10}) + \Psi(\Sigma_Q;{}^2\mathbf{8})), \quad (38)$$

$$\Psi(\Sigma_Q;{}^2\rho) = X_{1/2,0}\Phi_{1,0,1} = \frac{1}{\sqrt{2}}(\Psi(\Sigma_Q;{}^2\mathbf{10}) - \Psi(\Sigma_Q;{}^2\mathbf{8})), \quad (39)$$

$$\Psi(\Sigma_Q;{}^4\lambda) = X_{3/2,1}\Phi_{1,1,0} = \Psi(\Sigma_Q;{}^4\mathbf{8}) \quad (40)$$

for the Σ_Q baryons.

Generally, the λ modes appear lower in energy than the ρ modes and they do not mix with each other in the heavy-quark limit. The two states which are in the same mode but have different spin ($\Lambda_Q;{}^2\rho$, $\Lambda_Q;{}^4\rho$ and $\Sigma_Q;{}^2\lambda$, $\Sigma_Q;{}^4\lambda$) may mix even in the heavy-quark limit, because the light-quark spin-spin force is still alive in this limit. For intermediate heavy-quark masses, all these states may mix; the wave functions of energy eigenstates show how the mixings change as the heavy-quark mass increases.

A similar analysis can be done for other heavy-quark baryons. We tabulate, in Table VI, the λ- and ρ-mode

TABLE VI. The λ- and ρ-mode assignments of the P-wave excitations of Λ_Q, Σ_Q, Ξ_Q, Ξ_{QQ}, Ω_{QQ}, and Ω_{QQQ}. The quantum numbers are given in the Jacobi coordinate channel $c = 3$.

Flavor	ℓ	L	I	s	S	Mode	J
	0	1	1	0	1/2	${}^2\lambda$	$1/2^-, 3/2^-$
Λ_Q	1	0	1	1	1/2	${}^2\rho$	$1/2^-, 3/2^-$
	1	0	1	1	3/2	${}^4\rho$	$1/2^-, 3/2^-, 5/2^-$
	0	1	1	1	1/2	${}^2\lambda$	$1/2^-, 3/2^-$
Σ_Q	0	1	1	1	3/2	${}^4\lambda$	$1/2^-, 3/2^-, 5/2^-$
	1	0	1	0	1/2	${}^2\rho$	$1/2^-, 3/2^-$
	0	1	1	0	1/2	${}^2\lambda$	$1/2^-, 3/2^-$
	1	0	1	1	1/2	${}^2\rho$	$1/2^-, 3/2^-$
Ξ_Q	1	0	1	1	3/2	${}^4\rho$	$1/2^-, 3/2^-, 5/2^-$
	0	1	1	1	1/2	${}^2\lambda$	$1/2^-, 3/2^-$
	0	1	1	1	3/2	${}^4\lambda$	$1/2^-, 3/2^-, 5/2^-$
	1	0	1	0	1/2	${}^2\rho$	$1/2^-, 3/2^-$
	0	1	1	1	1/2	${}^2\lambda$	$1/2^-, 3/2^-$
Ξ_{QQ}	0	1	1	1	3/2	${}^4\lambda$	$1/2^-, 3/2^-, 5/2^-$
	1	0	1	0	1/2	${}^2\rho$	$1/2^-, 3/2^-$
	0	1	1	1	1/2	${}^2\lambda$	$1/2^-, 3/2^-$
Ω_{QQ}	0	1	1	1	3/2	${}^4\lambda$	$1/2^-, 3/2^-, 5/2^-$
	1	0	1	0	1/2	${}^2\rho$	$1/2^-, 3/2^-$
Ω_{QQQ}	0	1	1	1	1/2	${}^2\lambda$	$1/2^-, 3/2^-$
	1	0	1	0	1/2	${}^2\rho$	$1/2^-, 3/2^-$

classification of the P-wave heavy-quark baryons and their quantum numbers in the Jacobi coordinate channel $c = 3$.

In the heavy-quark limit, $m_Q \to \infty$, HQS symmetry becomes exact, where the spin degeneracy of $J = j \pm 1/2$ appears. In this limit, the light component $\boldsymbol{j} = \boldsymbol{J} - \boldsymbol{s}_Q$ and the heavy-quark spin $\boldsymbol{s}_Q$ are conserved independently, $[H, \boldsymbol{s}_Q] = 0 \to [H, \boldsymbol{J} - \boldsymbol{s}_Q] = [H, \boldsymbol{j}] = 0$. The basis in which j becomes diagonal can be written in terms of the Jacobi-coordinate basis states Eq. (17) for the channel $c = 3$ as

$$\begin{aligned}\Psi(qqQ; j; J) &= [[\chi_{1/2}(q)\chi_{1/2}(q)]_s \Phi_{\ell LI}]_j \chi_{1/2}(Q)]_J \\ &= \sum_S (-)^{(s+S+1/2)} \sqrt{(2S+1)(2j+1)} \\ &\quad \times \left\{ \begin{array}{ccc} 1/2 & s & S \\ I & J & j \end{array} \right\} [X_{S,s} \otimes \Phi_{I\ell L}]_J. \end{aligned} \tag{41}$$

III. RESULTS AND DISCUSSION

A. Energy spectra of single-heavy systems

We first discuss energy spectra of the single-charmed baryons, Λ_c, Σ_c, and Ω_c. The energies of the charmed baryons are listed in Table VII and are illustrated in Fig. 5. The mass of the lowest Λ_c is used to fix the charm quark mass m_c. The energy differences among the lowest $\Lambda_c(1/2^+)$, $\Sigma_c(1/2^+)$, and $\Sigma_c^*(3/2^+)$ states are given by $\Sigma_c(1/2^+) - \Lambda_c(1/2^+) = 175$ MeV (expt. 170 MeV), $\Sigma_c^*(3/2^+) - \Sigma_c(1/2^+) = 71$ MeV (expt. 65 MeV), which agree very well to the experimental data. The mass of the other single-charmed baryons are also well reproduced within a deviation of 50 MeV.

The energies of the lowest $\Lambda_c(1/2^-)$ and $\Lambda_c(3/2^-)$ states are consistent with the experimental data within 40 MeV, while the spin-orbit splitting between them is smaller than

TABLE VII. Calculated energy spectra and experimental results of Λ_c, Σ_c, and Ω_c.

Λ_c		
J^P	Theory (MeV)	Experiment (MeV)
$\frac{1}{2}^+$	2285	2285
	2857	
	3123	
$\frac{3}{2}^+$	2920	
	3175	
	3191	
$\frac{5}{2}^+$	2922	2881
	3202	
	3230	
$\frac{1}{2}^-$	2628	2595
	2890	
	2933	
$\frac{3}{2}^-$	2630	2628
	2917	
	2956	
$\frac{5}{2}^-$	2960	
	3444	
	3491	

Σ_c		
J^P	Theory (MeV)	Experiment (MeV)
$\frac{1}{2}^+$	2460	2455
	3029	
	3103	
$\frac{3}{2}^+$	2523	2518
	3065	
	3094	
$\frac{5}{2}^+$	3099	
	3114	
	3191	
$\frac{1}{2}^-$	2802	
	2826	
	2909	
$\frac{3}{2}^-$	2807	
	2837	
	2910	
$\frac{5}{2}^-$	2839	
	3316	
	3521	

Ω_c		
J^P	Theory (MeV)	Experiment (MeV)
$\frac{1}{2}^+$	2731	2698
	3227	
	3292	
$\frac{3}{2}^+$	2779	2768
	3257	
	3285	
$\frac{5}{2}^+$	3288	
	3299	
	3359	
$\frac{1}{2}^-$	3030	
	3048	
	3110	
$\frac{3}{2}^-$	3033	
	3056	
	3111	
$\frac{5}{2}^-$	3057	
	3477	
	3620	

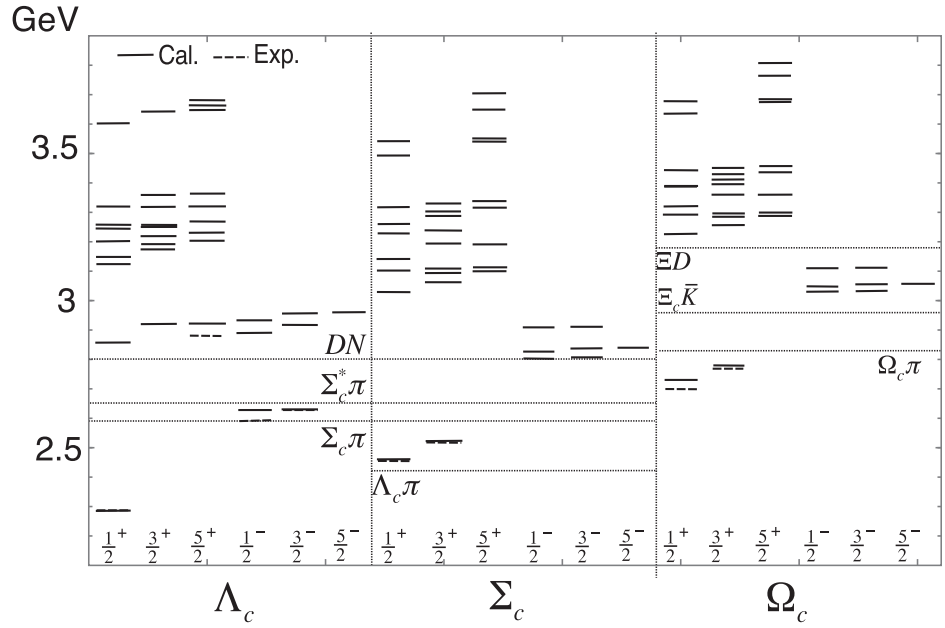

FIG. 5. Calculated energy spectra of Λ_c, Σ_c, and Ω_c for $1/2^+$, $3/2^+$, $5/2^+$, $1/2^-$, $3/2^-$, and $5/2^-$(solid line) together with experimental data (dashed line). Several thresholds are also shown by dotted lines.

TABLE VIII. Calculated energy spectra and experimental results of Λ_b, Σ_b, and Ω_b.

Λ_b		
J^P	Theory (MeV)	Experiment (MeV)
$\frac{1}{2}^+$	5618	5624
	6153	
	6467	
$\frac{3}{2}^+$	6211	
	6488	
	6511	
$\frac{5}{2}^+$	6212	
	6530	
	6539	
$\frac{1}{2}^-$	5938	5912
	6236	
	6273	
$\frac{3}{2}^-$	5939	5920
	6273	
	6285	
$\frac{5}{2}^-$	6289	
	6739	
	6786	

Σ_b		
J^P	Theory (MeV)	Experiment (MeV)
$\frac{1}{2}^+$	5823	5815
	6343	

(Table continued)

TABLE VIII. (*Continued*)

Σ_b		
J^P	Theory (MeV)	Experiment (MeV)
	6395	
$\frac{3}{2}^+$	5845	5835
	6356	
	6393	
$\frac{5}{2}^+$	6397	
	6402	
	6505	
$\frac{1}{2}^-$	6127	
	6135	
	6246	
$\frac{3}{2}^-$	6132	
	6141	
	6246	
$\frac{5}{2}^-$	6144	
	6592	
	6834	

Ω_b		
J^P	Theory (MeV)	Experiment (MeV)
$\frac{1}{2}^+$	6076	6048
	6517	
	6561	
$\frac{3}{2}^+$	6094	
	6528	

(Table continued)

TABLE VIII. (*Continued*)

Ω_b		
J^P	Theory (MeV)	Experiment (MeV)
	6559	
$\frac{5}{2}^+$	6561	
	6566	
	6657	
$\frac{1}{2}^-$	6333	
	6340	
	6437	
$\frac{3}{2}^-$	6336	
	6344	
	6438	
$\frac{5}{2}^-$	6345	
	6728	
	6919	

the observed ones. This tendency is also seen in the previous quark model calculations. One possible cause for the discrepancy is the coupling to the meson-baryon scattering states. As in the case of $\Lambda(1405)$, $\Lambda_c(2595)$ and $\Lambda_c(2628)$ may couple to DN and D^*N states [14,15]. Although the effects of the couplings may be smaller than the $\Lambda(1405)$ case due to the higher threshold of $D^{(*)}N$ continuum, the coupling may alter the spin-orbit splitting.

There are two observed states, $\Lambda_c(2940)$ and $\Sigma_c(2800)$, whose spin and parity have not been assigned. The present calculation indicates that $\Lambda_c(2940)$ can be assigned to one of the following states: $3/2_1^+$ (2920 MeV), $5/2_1^-$ (2960 MeV), $1/2_2^-$ (2890 MeV), $1/2_3^-$ (2933 MeV), $3/2_2^-$ (2917 MeV), and $3/2_3^-$ (2956 MeV), while $\Sigma_c(2800)$ may be assigned to one of $1/2_1^-$ (2802 MeV), $3/2_1^-$ (2807 MeV), $1/2_2^-$ (2826 MeV), $3/2_2^-$ (2837 MeV), and $5/2_1^-$ (2839 MeV). Here, J_n^P denotes the nth J^P state. Further experimental information, such as decay branching ratios and production rates, will be necessary to determine the quantum numbers of these states.

For $S=-2$ baryons, the lowest states of $\Omega_c(1/2^+)$ and $\Omega_c(3/2^+)$ have been experimentally observed. We underestimate the mass difference between them by about 20 MeV.

The masses of the single-bottom baryons are listed in Table VIII and illustrated in Fig. 6. The ground state Λ_b is fitted to the experimental data of the Particle Data Group. The mass differences among Λ_b, Σ_b, and Σ_b^* are $\Sigma_b(1/2^+)-\Lambda_b(1/2^+)=188$ MeV, $\Sigma_b^*(3/2^+)-\Sigma_b(1/2^+)=21$ MeV experimentally, while our calculation gives $\Sigma_b(1/2+)-\Lambda_b(1/2^+)=195$ MeV, and $\Sigma_b^*(3/2^+)-\Sigma_b(1/2^+)=22$ MeV. Thus, we find that the low-lying positive-parity states are reproduced within a 10-MeV deviation.

The negative-parity Λ_b states, $\Lambda_b(5912)$ and $\Lambda_b(5920)$, have been discovered recently. Their mass difference is about 8 MeV in experiment, and in our prediction it is 1 MeV. For $S=-2$ bottom baryons, $\Omega_b(1/2^+)$, our estimate of the mass is 6076 MeV, which is higher than the experimental value, 6015 MeV.

B. Energy spectra of double-heavy baryon systems

Tables IX and X and Figs. 7 and 8 show the calculated energy spectra and experimental data for double-heavy

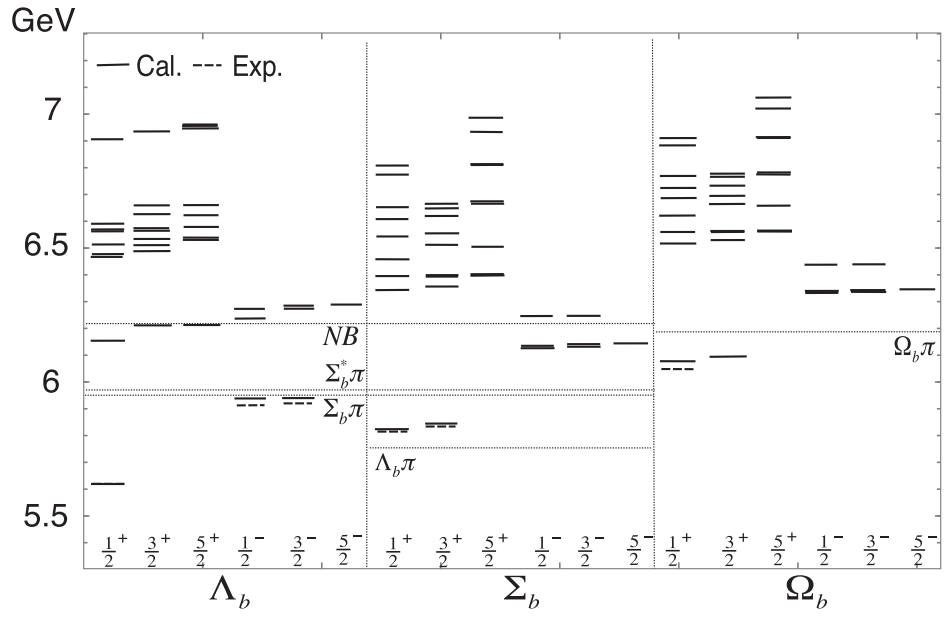

FIG. 6. Calculated energy spectra of Λ_b, Σ_b, and Ω_b for $1/2^+$, $3/2^+$, $5/2^+$, $1/2^-$, $3/2^-$, and $5/2^-$ (solid line) together with experimental data (dashed line). Several thresholds are also shown by dotted lines.

TABLE IX. Calculated energy spectra and experimental results of Ξ_{cc} and Ξ_{bb}.

Ξ_{cc}				
J^P	Theory (MeV)	Experiment (MeV)	[16]	[9]
$\frac{1}{2}^+$	3685	3512	$3603 \pm 15 \pm 16$	3674
	4079			4029
	4159			
$\frac{3}{2}^+$	3754		$3706 \pm 22 \pm 16$	3753
	4114			4042
	4131			
$\frac{5}{2}^+$	4115			4047
	4164			4091
	4348			
$\frac{1}{2}^-$	3947			3910
	4135			4074
	4149			
$\frac{3}{2}^-$	3949			3921
	4137			4078
	4159			
$\frac{5}{2}^-$	4163			4092
	4488			
	4534			

Ξ_{bb}		
J^P	Theory (MeV)	[9] (MeV)
$\frac{1}{2}^+$	10 314	10 340
	10 571	
	10 612	
$\frac{3}{2}^+$	10 339	10 367
	10 592	
	10 593	
$\frac{5}{2}^+$	10 592	10 676
	10 613	
	10 809	
$\frac{1}{2}^-$	10 476	10 493
	10 703	
	10 740	
$\frac{3}{2}^-$	10 476	10 495
	10 704	
	10 742	
$\frac{5}{2}^-$	10 759	10 713
	10 973	
	11 004	

TABLE X. Calculated energy spectra and experimental result of Ω_{cc} and Ω_{bb}.

Ω_{cc}			
J^P	Theory (MeV)	[16]	[9]
$\frac{1}{2}^+$	3832	$3704 \pm 5 \pm 16$	3815
	4227		4180
	4295		
$\frac{3}{2}^+$	3883	$3779 \pm 6 \pm 17$	3876
	4263		4188
	4265		
$\frac{5}{2}^+$	4264		4202
	4299		4232
	4410		
$\frac{1}{2}^-$	4086		4046
	4199		4135
	4210		
$\frac{3}{2}^-$	4086		4052
	4201		4140
	4218		
$\frac{5}{2}^-$	4220		4152
	4555		
	4600		

Ω_{bb}		
J^P	Theory (MeV)	[9]
$\frac{1}{2}^+$	10 447	10 454
	10 707	10 693
	10 744	
$\frac{3}{2}^+$	10 467	10 486
	10 723	10 721
	10 730	
$\frac{5}{2}^+$	10 729	10 720
	10 744	10 734
	10 937	
$\frac{1}{2}^-$	10 607	10 616
	10 796	10 763
	10 803	
$\frac{3}{2}^-$	10 608	10 619
	10 797	10 765
	10 805	
$\frac{5}{2}^-$	10 808	10 766
	11 028	
	11 059	

baryons. Lattice QCD [16,17] and quark models [9,18] predicted the masses of double-heavy baryons and variations among the model calculations to be large, compared to those in the single-heavy baryons.

The calculated mass of the lowest Ξ_{cc} state is 3685 MeV, which is much higher than the experimental observations by SELEX [19], 3519 MeV. However, the other experimental searches by *BABAR* [20], Belle [21], and LHCb [22] could not confirm this state. Our prediction is consistent with the recent Lattice QCD result as well as the other quark model calculations.

We predict that the lowest Ξ_{bb} state is $\Xi_{bb}(\frac{1}{2}^+) = 10\,314$ MeV followed by $\Xi_{bb}(\frac{3}{2}^+) = 10\,339$ MeV.

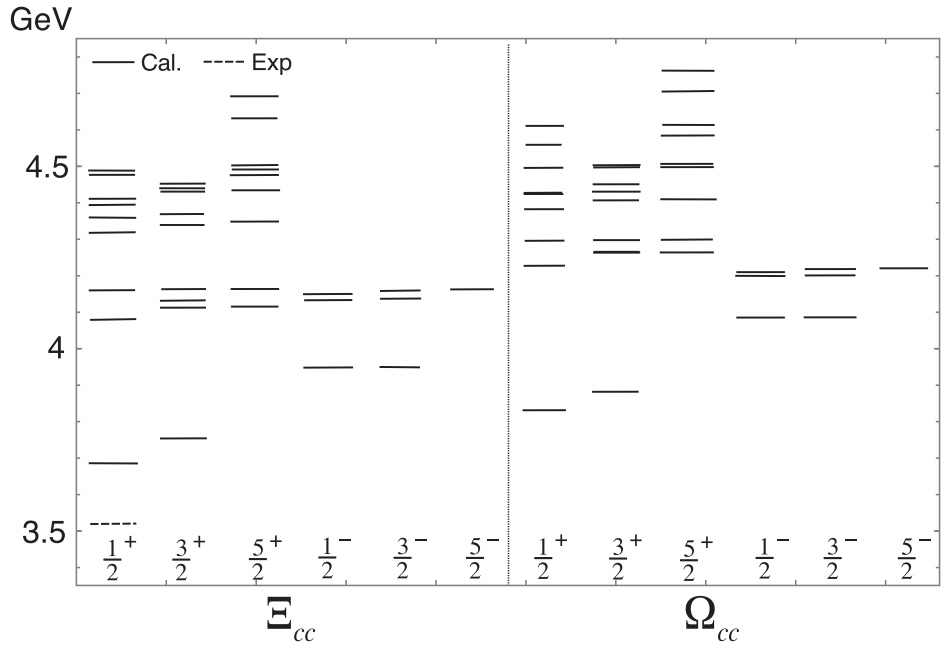

FIG. 7. Calculated energy spectra of Ξ_{cc} and Ω_{cc} for $1/2^+$, $3/2^+$, $5/2^+$, $1/2^-$, $3/2^-$, and $5/2^-$ (solid line) together with experimental data (dashed line).

C. λ-mode and ρ-mode structures in heavy-baryon systems

Now we compare the heavy-baryon spectra for the strange sector and the heavier sector (c and b) and clarify the quark dynamics in the heavy baryon. Strange baryons are conventionally analyzed by the $SU(3)_f$ symmetry. When the strange quark is replaced by a heavier quark, c or b, we can study the dynamics of the two light quarks, which may be regarded as a diquark. From this point of view, one sees two distinct excitation modes: λ and ρ modes. The λ-mode state is composed of the $(qq)_{\ell=0}$ diquark with $L = 1$ excitation relative to the heavy quark,

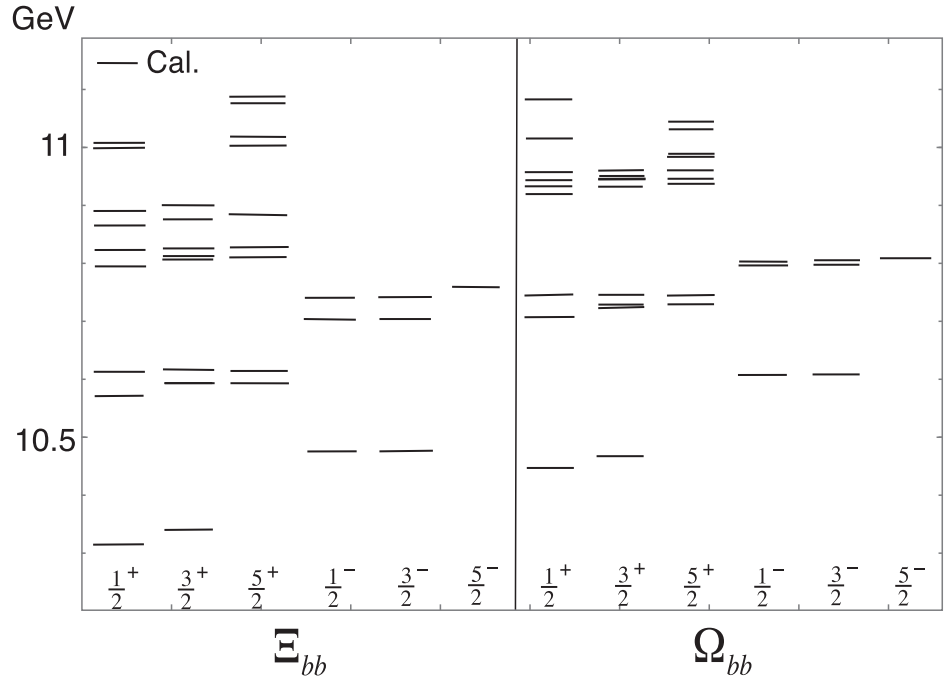

FIG. 8. Calculated energy spectra of Ξ_{bb} and Ω_{bb} for $1/2^+$, $3/2^+$, $5/2^+$, $1/2^-$, $3/2^-$, and $5/2^-$ (solid line) together with experimental data (dashed line).

Q, while the ρ-mode state has an excited diquark $(qq)_{\ell=1}$ in the $L=0$ orbit around Q.

As is discussed in Sec. I, the λ and ρ modes are largely mixed in the SU(3) limit in the light-quark sector. This mixing is induced mainly by the spin-spin interaction. Because the spin-dependent interaction for the heavy quark is weak, the λ and ρ modes are well separated for the charm and bottom baryons. Then, each P-wave state is dominated and characterized either by the λ mode or ρ mode.

In order to demonstrate these properties quantitatively, we change the heavy-quark mass, m_Q, from 300 MeV to 6 GeV and analyze the excitation energies and wave functions. Figure 9 shows the spectra of Λ_Q and Σ_Q as functions of m_Q. One sees that the splitting between the first and second $1/2^-$ state of Λ_Q increases rapidly from 100 MeV in the SU(3) limit to 300 MeV in the heavy-quark limit when m_Q increases. This behavior is due to the $\lambda-\rho$ splitting as demonstrated by the harmonic oscillator model (in Fig. 1). Namely, the lowest state becomes dominated by the λ mode as m_Q becomes large. This is confirmed in Fig. 10, where the λ- and ρ-mode probabilities of the lowest $1/2^-$ state are plotted as functions of m_Q. One sees that the state is almost purely in the λ mode at $m_Q \geq 1.5$ GeV; the λ dominance is seen even at $m_Q = 510$ MeV. As classified in Table VI, the quark model predicts seven P-wave Λ_Q excitations, $(1/2^-)^3$, $(3/2^-)^3$, $(5/2^-)$. They split into the $(1/2^-, 3/2^-)$ λ modes and $(1/2^-)^2$, $(3/2^-)^2$, $5/2^-$ ρ modes. In Fig. 9, one sees clear splitting ($\approx$350 MeV) of two low-lying λ modes and five higher ρ-mode states.

The P-wave Σ_Q has also seven states in the quark model, $(1/2^-)^3$, $(3/2^-)^3$, $(5/2^-)$. One sees that they are classified into the $(1/2)^2$, $(3/2^-)^2$, $(5/2^-)$ λ modes and $(1/2^-, 3/2^-)$

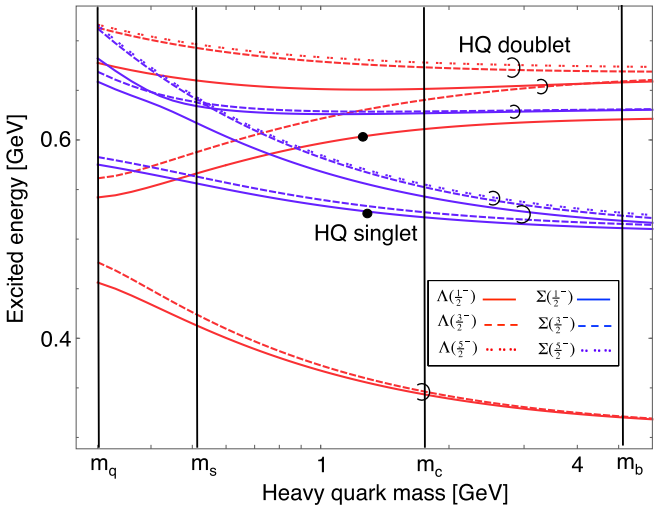

FIG. 9 (color online). Heavy-quark mass dependence of excited energies of the first, second, and third states for $1/2^-$ (solid line), $3/2^-$ (dashed line), and $5/2^-$ (double dotted line) of Λ_Q (red) and Σ_Q (blue). The bullet denotes a heavy-quark singlet. The pair within a half circle denotes a heavy-quark doublet.

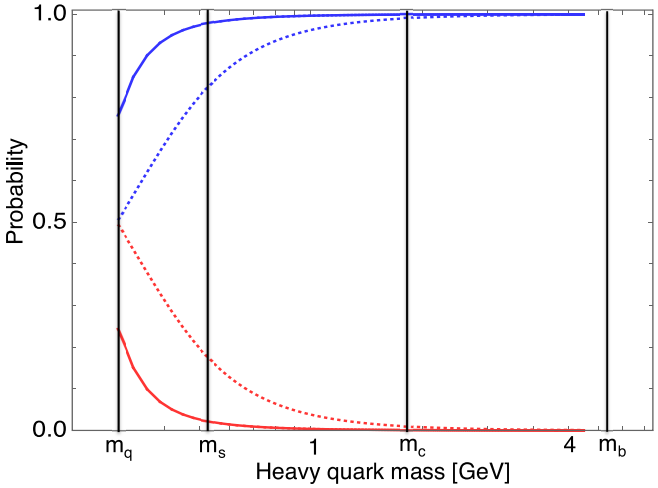

FIG. 10 (color online). The probability of the λ mode (blue line) and the ρ mode (red line) of $1/2^-$ for Σ_Q (dotted) and Λ_Q (solid).

ρ modes from Fig. 9. The λ and ρ modes are separated more slowly than Λ_Q as m_Q increases, and the λ dominance is seen at $m_Q \geq 1750$ MeV. The difference comes from the interaction between light quarks which forms the diquark. The diquark in Σ_Q has spin 1 and the spin-spin interaction is repulsive for the λ mode, while the ρ mode has a diquark state of spin 0 and the spin-spin interaction is attractive. Therefore, the difference between the excitation energies of the two modes is small compared to Λ_Q. Thus, the splitting between the excitation energies of two modes is larger for Λ_Q and smaller for Σ_Q compared with the case in which there is no spin-spin force, as we see in Sec. I. As a result, the change of the probability of two modes in the Σ_Q case is more slow than the Λ_Q case, as shown in Fig. 10.

In the case of double-heavy baryon, the λ-mode state is composed of the $(QQ)_{\ell=0}$ heavy diquark with the light quark q, while the ρ-mode state has the excited heavy diquark $(QQ)_{\ell=1}$ in the $L=0$ orbit around q. The combinations of angular momentum are the same as the Σ_Q case, which is shown in Table VI, but the behavior of the λ and ρ modes are different because Ξ_{QQ} or Ω_{QQ} contains a heavy diquark. As mentioned in Sec. I, ω_λ is larger than ω_ρ for the P-wave double-heavy baryons and thus ρ modes are dominant. This is shown in Figs. 11 and 12. One sees that the $(1/2)^2$, $(3/2^-)^2$, $(5/2^-)$ λ modes and the $(1/2^-, 3/2^-)$ ρ modes split in the heavy-quark region in Fig. 11, and the ρ modes become dominant for the lowest states at $m_Q \geq m_c$ in Fig. 12.

D. Heavy baryons in the heavy-quark limit

In this subsection, we investigate the behavior of the single-heavy baryons in the heavy-quark limit. We decompose the wave functions of the P-wave single-heavy baryons into the parts with different light-spin

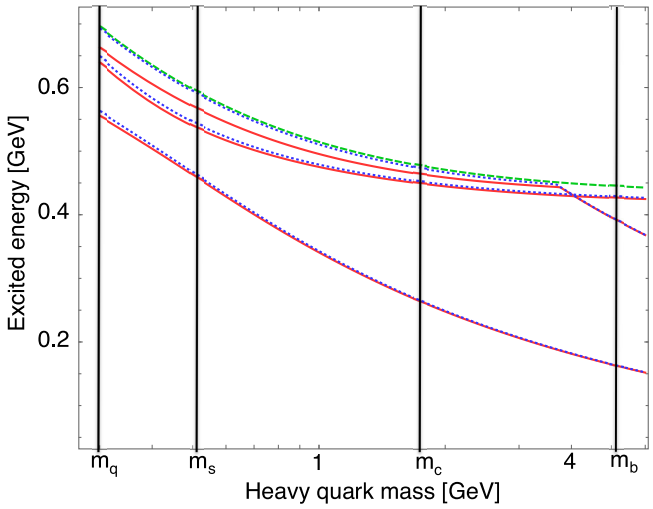

FIG. 11 (color online). Heavy-quark mass dependence of excited energies of the first, second, and third state for $1/2^-$ (red solid line), $3/2^-$ (blue dotted line), and $5/2^-$ (green dashed line) of Ξ_{QQ}.

component j as

$$\Phi_{\Lambda_Q}^{J=1/2,M}(\boldsymbol{\rho},\boldsymbol{\lambda}) = \phi_{\Lambda_Q,j=0}^{J=1/2,M}(\boldsymbol{\rho},\boldsymbol{\lambda}) + \phi_{\Lambda_Q,j=1}^{J=1/2,M}(\boldsymbol{\rho},\boldsymbol{\lambda}), \tag{42}$$

$$\Phi_{\Lambda_Q}^{J=3/2,M}(\boldsymbol{\rho},\boldsymbol{\lambda}) = \phi_{\Lambda_Q,j=1}^{J=3/2,M}(\boldsymbol{\rho},\boldsymbol{\lambda}) + \phi_{\Lambda_Q,j=2}^{J=3/2,M}(\boldsymbol{\rho},\boldsymbol{\lambda}), \tag{43}$$

$$\Phi_{\Sigma_Q}^{J=1/2,M}(\boldsymbol{\rho},\boldsymbol{\lambda}) = \phi_{\Sigma_Q,j=0}^{J=1/2,M}(\boldsymbol{\rho},\boldsymbol{\lambda}) + \phi_{\Sigma_Q,j=1}^{J=1/2,M}(\boldsymbol{\rho},\boldsymbol{\lambda}), \tag{44}$$

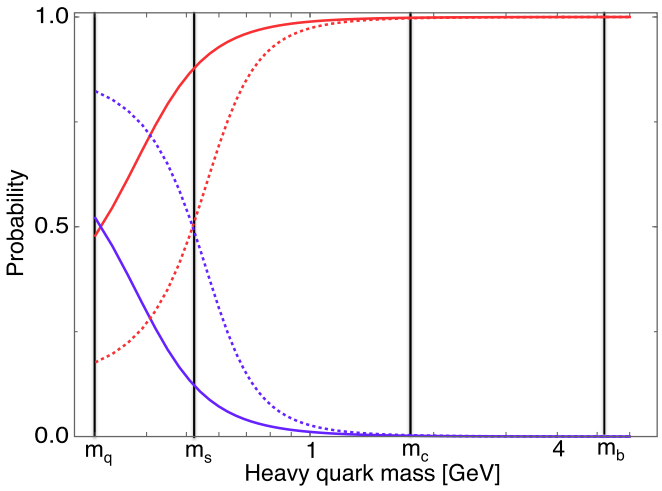

FIG. 12 (color online). The probability of the λ mode (blue line) and the ρ mode (red line) of $1/2^-$ for Ξ_{QQ} (solid) and Ω_{QQ} (dotted).

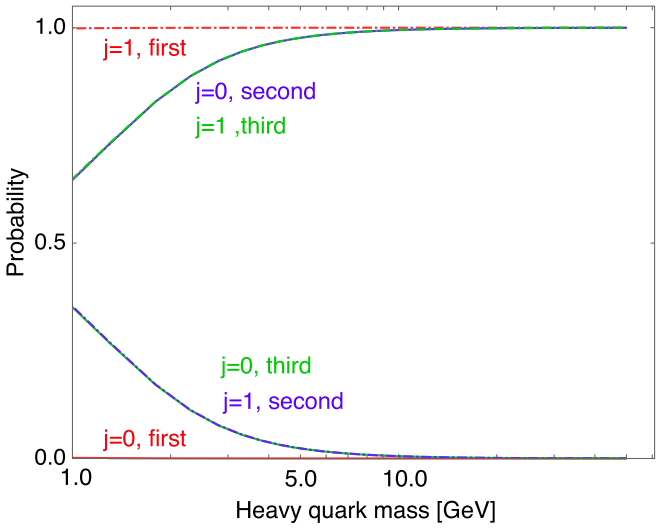

FIG. 13 (color online). The probabilities of $j = 0$ (solid line) and $j = 1$ (dot-dashed line) for $\Lambda(1/2^-)$. Red, blue, and green lines show the first, second, and third state, respectively.

$$\Phi_{\Sigma_Q}^{J=3/2,M}(\boldsymbol{\rho},\boldsymbol{\lambda}) = \phi_{\Sigma_Q,j=1}^{J=3/2,M}(\boldsymbol{\rho},\boldsymbol{\lambda}) + \phi_{\Sigma_Q,j=2}^{J=3/2,M}(\boldsymbol{\rho},\boldsymbol{\lambda}). \tag{45}$$

Here, we take into account only the channel $c = 3$ of the Jacobi coordinates, given in Fig. 2. The relation between the representation Eqs. (42)–(45) and Eq. (15) is shown in the Appendix. The heavy-quark mass dependences of the probabilities of each j state are shown in Figs. 13–16 (see the Appendix for the definition). The mixings between $j = 0$ and $j = 1$ or $j = 1$ and $j = 2$ above 1 GeV are negligible for the first state of $\Lambda_Q(1/2^-)$ and $\Lambda_Q(3/2^-)$ and the third state of $\Sigma_Q(1/2^-)$ and $\Sigma_Q(3/2^-)$, which correspond to the

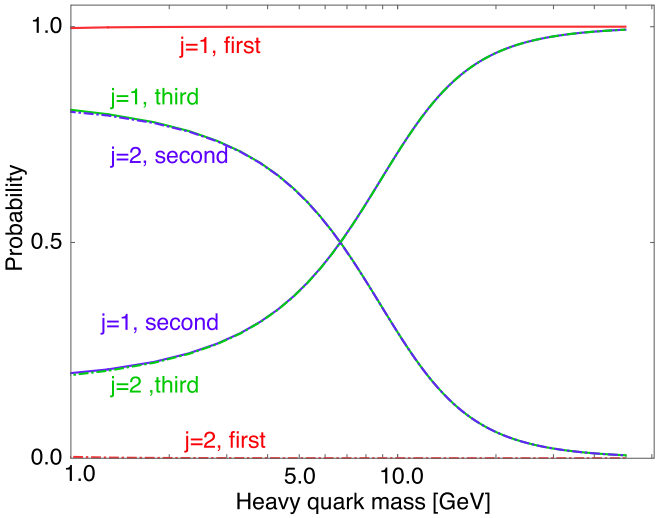

FIG. 14 (color online). The probabilities of $j = 1$ (solid line) and $j = 2$ (dot-dashed line) for $\Lambda(3/2^-)$. Red, blue, and green lines show the first, second, and third state, respectively.

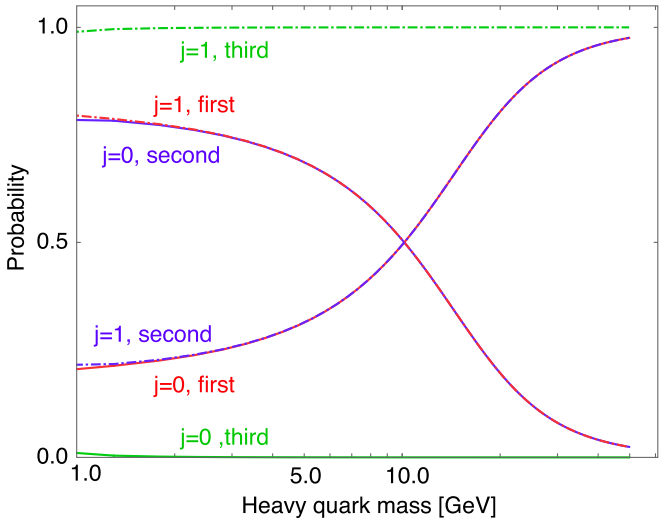

FIG. 15 (color online). The probabilities of $j = 0$ (solid line) and $j = 1$ (dot-dashed line) for $\Sigma(1/2^-)$. Red, blue, and green lines show the first, second, and third state, respectively.

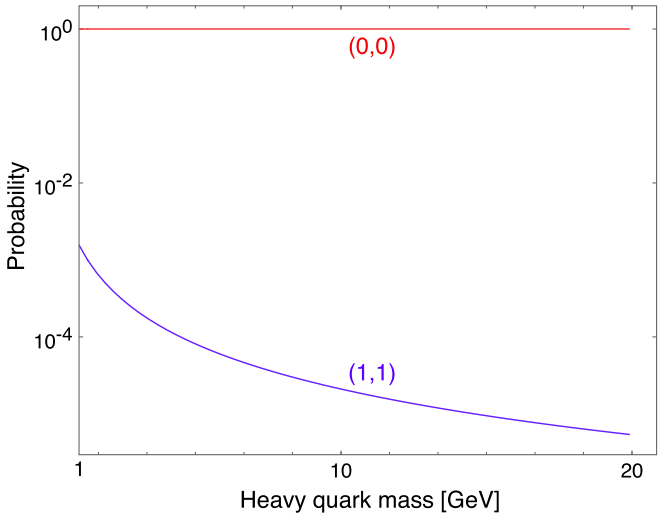

FIG. 17 (color online). The heavy-quark mass dependences of the probabilities of the S-wave (0.0) component (red line) and (1,1) component (blue line) for $\Lambda(1/2^+_1)$.

red lines in Figs. 13–14 and the green lines in Figs. 15–16. This is because these states are isolated from the other states, as shown in Fig. 9. For the other state, two different j components (five λ modes of Σ_Q and five ρ modes of Λ_Q) still mix in the charm and bottom mass region, because they lie close to each other within 50 MeV (see Fig. 9). Above $m_Q = 14$ GeV, one sees no mixing between different j components. In summary, one finds that the second $1/2^-$ state of Λ_Q and the first $1/2^-$ state of $1/2^-$ of Σ_Q are the $j = 0$ singlet state. All the other states belong to doublets, $(1/2^-_1, 3/2^-_1)$, $(1/2^-_3, 3/2^-_2)$, and $(3/2^-_3, 5/2^-_1)$ for Λ_Q and $(1/2^-_2, 3/2^-_1)$, $(3/2^-_2, 5/2^-_1)$, and $(1/2^-_3, 3/2^-_2)$ for Σ_Q, as shown in Fig. 9.

We next discuss the positive-parity states. We focus on the first six positive-parity states of single-heavy baryons, corresponding to the states below 3.0 GeV in the charm sector (see Fig. 5). They consist of the S-wave $[(L, \ell) = (0, 0)]$ component, the (1,1) component, the (2,0) component (ρ mode), and the (0,2) component (λ mode). Figures 17–22 show the probabilities of the each component in the total wave function. One sees that one component becomes dominant above $m_Q = 1$ GeV. The (0,0) component is dominant for $\Lambda_Q(1/2^+_1)$, $\Lambda_Q(1/2^+_2)$, $\Sigma_Q(1/2^+_1)$, and $\Sigma_Q(1/2^+_2)$ and the (2,0) component (λ mode) is dominant for $\Lambda_Q(3/2^+_1)$, $\Lambda_Q(5/2^+_1)$ above 1 GeV (see Figs. 17–22). The lowest

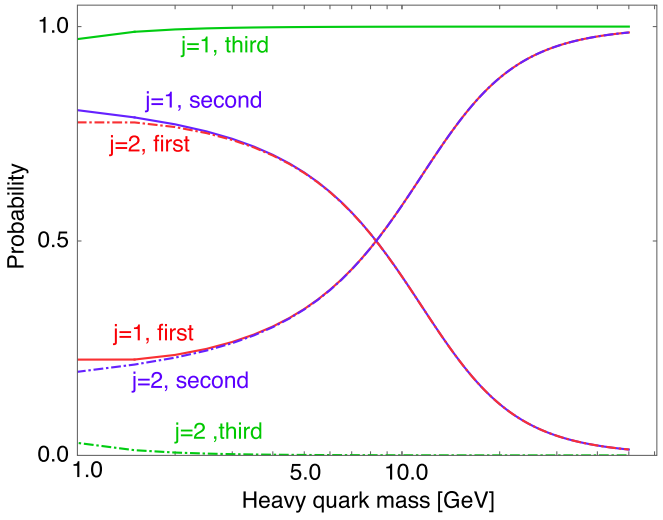

FIG. 16 (color online). The probabilities of $j = 1$ (solid line) and $j = 2$ (dot-dashed line) for $\Sigma(3/2^-)$. Red, blue, and green lines show the first, second, and third state, respectively.

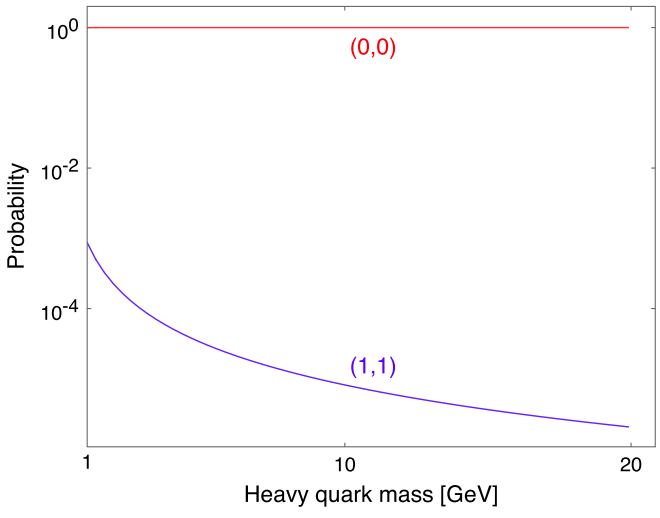

FIG. 18 (color online). The heavy-quark mass dependences of the probabilities of the S-wave (0,0) component (red line) and the (1,1) component (blue line) for $\Lambda(1/2^+_2)$.

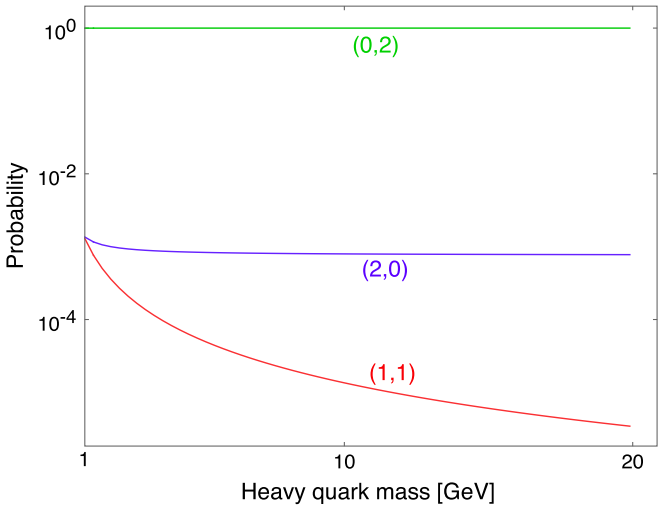

FIG. 19 (color online). The heavy-quark mass dependences of the probabilities of the (1,1) component (red line), the (2,0) component (blue line), and the (0,2) component (green line) for $\Lambda(3/2_1^+)$.

six states in the heavy-quark region can be written as follows:

$$\Phi_{\Lambda_Q}^{J_n=1/2_1,M}(\boldsymbol{\rho},\boldsymbol{\lambda}) = \phi_{\Lambda_Q,j=0}^{J_n=1/2_1^+,M}(\boldsymbol{\rho},\boldsymbol{\lambda}), \tag{46}$$

$$\Phi_{\Lambda_Q}^{J_n=1/2_2,M}(\boldsymbol{\rho},\boldsymbol{\lambda}) = \phi_{\Lambda_Q,j=0}^{J_n=1/2_2,M}(\boldsymbol{\rho},\boldsymbol{\lambda}), \tag{47}$$

$$\Phi_{\Lambda_Q}^{J_n=3/2_1,M}(\boldsymbol{\rho},\boldsymbol{\lambda}) = \phi_{\Lambda_Q,j=2}^{J_n=3/2_1,M}(\boldsymbol{\rho},\boldsymbol{\lambda}), \tag{48}$$

$$\Phi_{\Lambda_Q}^{J_n=5/2_1,M}(\boldsymbol{\rho},\boldsymbol{\lambda}) = \phi_{\Lambda_Q,j=2}^{J_n=5/2_1,M}(\boldsymbol{\rho},\boldsymbol{\lambda}), \tag{49}$$

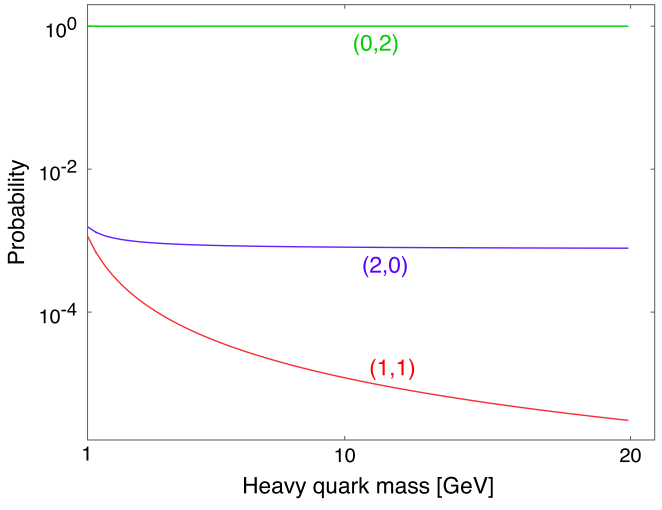

FIG. 20 (color online). The heavy-quark mass dependences of the probabilities of the (1,1) component (red line), the (2,0) component (blue line), and the (0,2) component (green line) for $\Lambda(5/2_1^+)$.

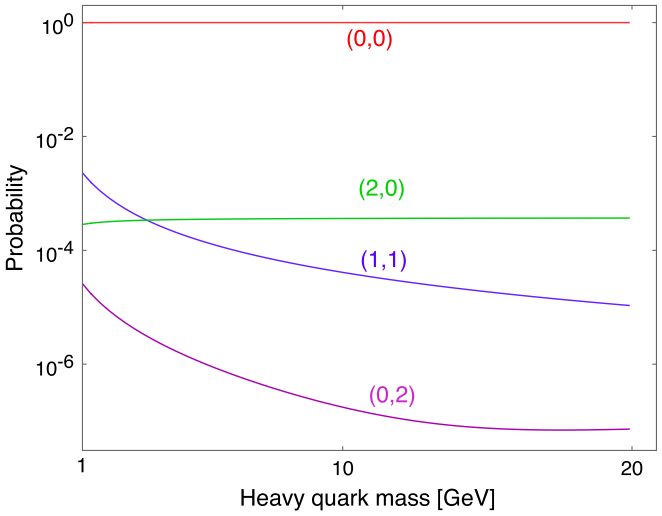

FIG. 21 (color online). The heavy-quark mass dependences of the probabilities of the S-wave (0,0) component (red line), the (1,1) component (blue line), the (2,0) component (green line), and the (0,2) component (violet line) for $\Sigma(1/2_1^+)$.

$$\Phi_{\Sigma_Q}^{J_n=1/2_1,M}(\boldsymbol{\rho},\boldsymbol{\lambda}) = \phi_{\Sigma_Q,j=1}^{J_n=1/2_1,M}(\boldsymbol{\rho},\boldsymbol{\lambda}), \tag{50}$$

$$\Phi_{\Sigma_Q}^{J_n=3/2_1,M}(\boldsymbol{\rho},\boldsymbol{\lambda}) = \phi_{\Sigma_Q,j=1}^{J_n=3/2_1,M}(\boldsymbol{\rho},\boldsymbol{\lambda}), \tag{51}$$

where we use Eq. (41) to transform the bases. There are two doublet pairs $[\Lambda_Q(3/2_1^+),\ \Lambda_Q(5/2_1^+)]$ $(j=2)$, $[\Sigma_Q(1/2_1^+),\ \Sigma_Q(3/2_1^+)]$ $(j=1)$ and two singlet states $\Lambda_Q(1/2_1^+)$, $\Lambda_Q(1/2_2^+)$ in the heavy-quark limit. Mixings of different j components of the wave function are negligible even in the charm-quark region.

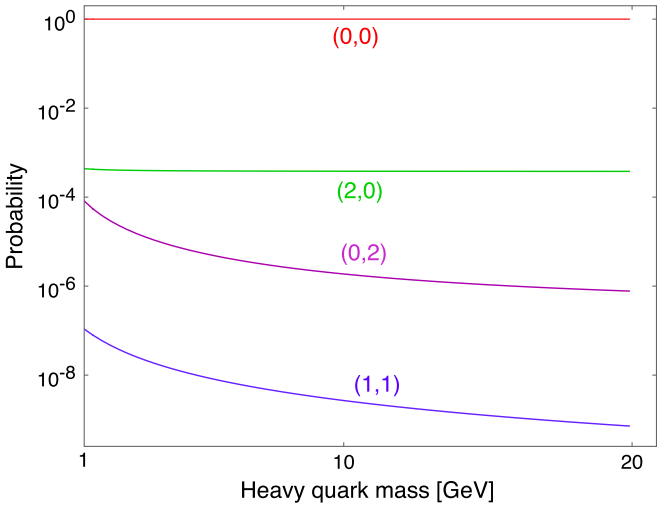

FIG. 22 (color online). The heavy-quark mass dependences of the probabilities of the S-wave ($l=0$, $L=0$) component (red line), the (1,1) component (blue line), the (2,0) component (green line), and the (0,2) component (violet line) for $\Sigma(3/2_1^+)$.

IV. SUMMARY

We have studied the spectrum of the single- and double-heavy baryons and discussed their structures within the framework of a constituent quark model. The potential parameters are determined so as to reproduce the energies of the lowest states: $\Lambda(1/2^+)$, $\Sigma(1/2^+)$, $\Sigma(3/2^+)$, $\Lambda(1/2^-)$, $\Lambda(3/2^-)$, $\Lambda_c(1/2^+)$, and $\Lambda_b(1/2^+)$. In the analysis of the baryon wave functions, we have focused on the two characteristic excited modes and investigated their probabilities as functions of the heavy-quark mass. To obtain the precise energy eigenvalues of excited states, we employ the Gaussian expansion method, which is one of the best methods for three- and four-body bound states. We have obtained the following:

(1) Masses of the known Λ_Q, Σ_Q, and Ω_Q are in good agreement with the observed data within 50 MeV. Then, we predicted that observed $\Sigma_c(2800)$ can be assigned to the $1/2^-_1$, $3/2^-_1$, $1/2^-_2$, $3/2^-_2$, and $5/2^-_1$ states, and Λ_c to the $3/2^+_1$, $5/2^-_1$, $1/2^-_2$, $1/2^-_3$, $3/2^-_2$, and $3/2^-_3$ states.

(2) In the heavy-quark limit, we find six doublets and two singlets for the P-wave single-heavy baryons (see Fig. 9) and two doublets and two singlets for the first six states of positive-parity single-heavy baryons. In the charm sector, the mass differences of these heavy-quark spin doublets are less than 30 MeV and in the bottom sector, the differences reduce to less than 10 MeV.

(3) For the double-heavy baryons, we predict that the mass of the ground Ξ_{cc} state is $\Xi_{cc}(3685)$. This result is consistent with the recent Lattice QCD calculations within 50 MeV. Experimentally, it was reported that a double- charmed baryon was found at the mass 3512 MeV [19]. However, other experimental groups, including the LHC and Belle Collaborations, have not yet succeeded in the observing the state.

(4) We have investigated the dependences on the heavy-quark mass m_Q of the λ and ρ modes to see the features of the negative-parity states. Mixings of the ρ and λ modes are suppressed and only one mode dominates. This is because the spin-spin interaction, which mainly causes the mixing, becomes small in the heavy-quark region. It would be useful, in future work, to clarify what physical quantities are sensitive the differences of the two modes. One possibility is decay patterns, as it is conjectured that the λ-mode states decay dominantly to a light baryon and a heavy meson, while the ρ-mode states decay mostly into a light meson and a heavy baryon. More studies of the decays and productions of these heavy baryons will be useful in order to further verify these structures.

ACKNOWLEDGMENTS

The authors would like to thank Dr. Shigehiro Yasui and Dr. Hiroyuki Noumi for valuable discussions. This work was supported in part by JSPS KAKENHI Grants No. 25247036, No. 24250294, and No. 26400273. T. Y. acknowledges the Junior Research Associate scholarship at RIKEN. The numerical calculations were carried out on SR16000 at YITP in Kyoto University.

APPENDIX: THE TRANSFORMATION OF THE BASES

We discuss the wave function in the heavy-quark limit in this appendix. For the single-heavy baryons, we take only the channel $c = 3$ of the Jacobi coordinate given in Fig. 2. The P-wave wave functions of the Λ_Q and Σ_Q baryons are given by the sum of the λ-mode ($^{2S+1}\lambda = {}^2\lambda,\ {}^4\lambda$) and ρ-mode ($^{2S+1}\rho = {}^2\rho,\ {}^4\rho$) components as follows:

$$\Phi^{JM}_{\Lambda_Q}(\boldsymbol{\rho},\boldsymbol{\lambda}) = \psi^{\Lambda_Q}_{^2\rho}\sum_{(n,N)} C^{^2\rho}_{n,N}\phi_{n,N}(\rho,\lambda) + \psi^{\Lambda_Q}_{^4\rho}\sum_{(n,N)} C^{^4\rho}_{n,N}\phi_{n,N}(\rho,\lambda) + \psi^{\Lambda_Q}_{^2\lambda}\sum_{(n,N)} C^{^2\lambda}_{n,N}\phi_{n}(\rho,\lambda), \tag{A1}$$

$$\Phi^{JM}_{\Sigma_Q}(\boldsymbol{\rho},\boldsymbol{\lambda}) = \psi^{\Sigma_Q}_{^2\lambda}\sum_{(n,N)} C^{^2\lambda}_{n,N}\phi_{n}(\rho,\lambda) + \psi^{\Sigma_Q}_{^4\lambda}\sum_{(n,N)} C^{^4\lambda}_{n}\phi_{n,N}(\rho,\lambda) + \psi^{\Sigma_Q}_{^2\rho}\sum_{(n,N)} C^{^2\rho}_{n,N}\phi_{n,N}(\rho,\lambda). \tag{A2}$$

Here we extract the parts of the spin and orbital angular momenta for each mode as

$$\psi^{\Lambda_Q}_{^2\rho} = [X_{S=1/2,1}[Y_{\ell=1}(\hat{\boldsymbol{\rho}})Y_{L=0}(\hat{\boldsymbol{\lambda}})]_{I=1}]_{JM}, \tag{A3}$$

$$\psi^{\Lambda_Q}_{^4\rho} = [X_{S=3/2,1}[Y_{\ell=1}(\hat{\boldsymbol{\rho}})Y_{L=0}(\hat{\boldsymbol{\lambda}})]_{I=1}]_{JM}, \tag{A4}$$

$$\psi^{\Lambda_Q}_{^2\lambda} = [X_{S=1/2,0}[Y_{\ell=0}(\hat{\boldsymbol{\rho}})Y_{L=1}(\hat{\boldsymbol{\lambda}})]_{I=1}]_{JM}, \tag{A5}$$

$$\psi^{\Sigma_Q}_{^2\lambda} = [X_{S=1/2,1}[Y_{\ell=0}(\hat{\boldsymbol{\rho}})Y_{L=1}(\hat{\boldsymbol{\lambda}})]_{I=1}]_{JM}, \tag{A6}$$

$$\psi^{\Sigma_Q}_{^4\lambda} = [X_{S=3/2,1}[Y_{\ell=0}(\hat{\boldsymbol{\rho}})Y_{L=1}(\hat{\boldsymbol{\lambda}})]_{I=1}]_{JM}, \tag{A7}$$

$$\psi^{\Sigma_Q}_{^2\rho} = [X_{S=1/2,0}[Y_{\ell=1}(\hat{\boldsymbol{\rho}})Y_{L=0}(\hat{\boldsymbol{\lambda}})]_{I=1}]_{JM}. \tag{A8}$$

Then, the corresponding radial parts are expanded by the Gaussian basis as

$$\phi_{n,N}(\rho,\lambda) = N_{n\ell} N_{NL} \rho^{\ell} e^{-\beta_n \rho^2} \lambda^L e^{-\gamma_N \lambda^2}, \tag{A9}$$

where $N_{nl}(N_{NL})$ is the normalization constant. As discussed in Sec. III C, the light-spin component j is conserved in the heavy-quark limit. Therefore, we transform the bases into those which diagonalize j. We use Eq. (41) to transform the bases, and obtain

$$\psi^{\Lambda_Q}_{2_\rho} = \sqrt{\frac{1}{3}}\psi_{j=0,s=1} - \sqrt{\frac{2}{3}}\psi_{j=1,s=1}, \tag{A10}$$

$$\psi^{\Lambda_Q}_{4_\rho} = \sqrt{\frac{2}{3}}\psi_{j=0,s=1} + \sqrt{\frac{1}{3}}\psi_{j=1,s=1}, \tag{A11}$$

$$\psi^{\Lambda_Q}_{2_\lambda} = -\psi_{j=1,s=0}, \tag{A12}$$

$$\psi^{\Sigma_Q}_{2_\lambda} = \sqrt{\frac{1}{3}}\psi_{j=0,s=1} - \sqrt{\frac{2}{3}}\psi_{j=1,s=1}, \tag{A13}$$

$$\psi^{\Sigma_Q}_{4_\lambda} = \sqrt{\frac{2}{3}}\psi_{j=0,s=1} + \sqrt{\frac{1}{3}}\psi_{j=1,s=1}, \tag{A14}$$

$$\psi^{\Sigma_Q}_{2_\rho} = -\psi_{j=1,s=0} \tag{A15}$$

for $J = 1/2^-$ and

$$\psi^{\Lambda_Q}_{2_\rho} = -\sqrt{\frac{1}{6}}\psi_{j=1,s=1} + \sqrt{\frac{5}{6}}\psi_{j=2,s=1}, \tag{A16}$$

$$\psi^{\Lambda_Q}_{4_\rho} = -\sqrt{\frac{5}{6}}\psi_{j=1,s=1} - \sqrt{\frac{1}{6}}\psi_{j=2,s=1}, \tag{A17}$$

$$\psi^{\Lambda_Q}_{2_\lambda} = \psi_{j=1,s=0}, \tag{A18}$$

$$\psi^{\Sigma_Q}_{2_\lambda} = -\sqrt{\frac{1}{6}}\psi_{j=1,s=1} + \sqrt{\frac{5}{6}}\psi_{j=2,s=1}, \tag{A19}$$

$$\psi^{\Sigma_Q}_{4_\lambda} = -\sqrt{\frac{5}{6}}\psi_{j=1,s=1} - \sqrt{\frac{1}{6}}\psi_{j=2,s=1}, \tag{A20}$$

$$\psi^{\Sigma_Q}_{2_\rho} = \psi_{j=1,s=0} \tag{A21}$$

for $J = 3/2^-$, where

$$\psi_{j,s} = [[[\chi_{1/2}(q)\chi_{1/2}(q)]_s [Y(\hat{\boldsymbol{\rho}})_\ell Y(\hat{\boldsymbol{\lambda}})_L]_I]_j \chi_{1/2}(Q)]_J. \tag{A22}$$

By using Eqs. (A3)–(A8), Eq. (A1) and Eq. (A2) are transformed into the bases that are characterized by j, as follows:

(i) $\Lambda_Q(1/2^-, 3/2^-)$:

$$\phi^{J=1/2,M}_{\Lambda_Q,j=0}(\boldsymbol{\rho},\boldsymbol{\lambda}) = \psi_{j=0,s=1}\left(\sqrt{\frac{1}{3}}\sum_{(n,N)} C^{2\rho}_{n,N}\phi_{n,N}(\rho,\lambda) + \sqrt{\frac{2}{3}}\sum_{(n,N)} C^{4\rho}_{n,N}\phi_{n,N}(\rho,\lambda)\right) - \psi_{j=0,s=0}\sum_{(n,N)} C^{2\lambda}_{n,N}\phi_{n,N}(\rho,\lambda), \tag{A23}$$

$$\phi^{J=1/2,M}_{\Lambda_Q,j=1}(\boldsymbol{\rho},\boldsymbol{\lambda}) = \psi_{j=1,s=1}\left(-\sqrt{\frac{2}{3}}\sum_{(n,N)} C^{2\rho}_{n,N}\phi_{n,N}(\rho,\lambda) + \sqrt{\frac{1}{3}}\sum_{(n,N)} C^{4\rho}_{n,N}\phi_{n,N}(\rho,\lambda)\right), \tag{A24}$$

$$\phi^{J=3/2,M}_{\Lambda_Q,j=1}(\boldsymbol{\rho},\boldsymbol{\lambda}) = \psi_{j=1,s=1}\left(-\sqrt{\frac{1}{6}}\sum_{(n,N)} C^{2\rho}_{n,N}\phi_{n,N}(\rho,\lambda) - \sqrt{\frac{5}{6}}\sum_{(n,N)} C^{4\rho}_{n,N}\phi_{n,N}(\rho,\lambda)\right) + \psi_{j=1,s=0}\sum_{(n,N)} C^{2\lambda}_{n,N}\phi_{n,N}(\rho,\lambda), \tag{A25}$$

$$\phi^{J=3/2,M}_{\Lambda_Q,j=2}(\boldsymbol{\rho},\boldsymbol{\lambda}) = \psi_{j=2,s=1}\left(\sqrt{\frac{5}{6}}\sum_{(n,N)} C^{2\rho}_{n,N}\phi_{n,N}(\rho,\lambda) - \sqrt{\frac{1}{6}}\sum_{(n,N)} C^{4\rho}_{n,N}\phi_{n,N}(\rho,\lambda)\right). \tag{A26}$$

(ii) $\Sigma_Q(1/2^-, 3/2^-)$:

$$\phi^{J=1/2,M}_{\Sigma_Q,j=0}(\boldsymbol{\rho},\boldsymbol{\lambda}) = \psi_{j=0,s=1}\left(\sqrt{\frac{1}{3}}\sum_{(n,N)} C^{2\lambda}_{n,N}\phi_{n,N}(\rho,\lambda) + \sqrt{\frac{2}{3}}\sum_{(n,N)} C^{4\lambda}_{n,N}\phi_{n,N}(\rho,\lambda)\right) - \psi_{j=0,s=0}\sum_{(n,N)} C^{2\rho}_{n,N}\phi_{n,N}(\rho,\lambda), \tag{A27}$$

$$\phi^{J=1/2,M}_{\Sigma_Q,j=1}(\boldsymbol{\rho},\boldsymbol{\lambda}) = \psi_{j=1,s=1}\left(-\sqrt{\frac{2}{3}}\sum_{(n,N)} C^{2\lambda}_{n,N}\phi_{n,N}(\rho,\lambda) + \sqrt{\frac{1}{3}}\sum_{(n,N)} C^{4\lambda}_{n,N}\phi_{n,N}(\rho,\lambda)\right), \tag{A28}$$

$$\phi^{J=3/2,M}_{\Sigma_Q,j=1}(\boldsymbol{\rho},\boldsymbol{\lambda}) = \psi_{j=1,s=1}\left(-\sqrt{\frac{1}{6}}\sum_{(n,N)} C^{^2\lambda}_{n,N}\phi_{n,N}(\rho,\lambda) - \sqrt{\frac{5}{6}}\sum_{(n,N)} C^{^4\lambda}_{n,N}\phi_{n,N}(\rho,\lambda)\right) + \psi_{j=1,s=0}\sum_{(n,N)} C^{^2\rho}_{n,N}\phi_{n,N}(\rho,\lambda), \tag{A29}$$

$$\phi^{J=3/2,M}_{\Sigma_Q,j=2}(\boldsymbol{\rho},\boldsymbol{\lambda}) = \psi_{j=2,s=1}\left(\sqrt{\frac{5}{6}}\sum_{(n,N)} C^{^2\lambda}_{n,N}\phi_{n,N}(\rho,\lambda) - \sqrt{\frac{1}{6}}\sum_{(n,N)} C^{^4\lambda}_{n,N}\phi_{n,N}(\rho,\lambda)\right). \tag{A30}$$

[1] M. Voloshin, Charmonium, Prog. Part. Nucl. Phys. **61**, 455 (2008).

[2] S. Ohkoda, Y. Yamaguchi, S. Yasui, K. Sudoh, and A. Hosaka, Exotic mesons with hidden bottom near thresholds, Phys. Rev. D **86**, 014004 (2012).

[3] R. Aaij *et al.* (LHCb Collaboration), Observation of $J/\psi p$ Resonances Consistent with Pentaquark States in $\Lambda_b^0 \to J/\psi K^- p$ Decays, Phys. Rev. Lett. **115**, 072001 (2015).

[4] S. H. Lee, S. Yasui, W. Liu, and C. M. Ko, Charmed exotics in heavy ion collisions, Eur. Phys. J. C **54**, 259 (2008).

[5] L. Maiani, F. Piccinini, A. D. Polosa, and V. Riquer, Diquark-antidiquark states with hidden or open charm and the nature of X(3872), Phys. Rev. D **71**, 014028 (2005).

[6] A. Selem and F. Wilczek, Hadron systematics and emergent diquarks, arXiv:hep-ph/0602128.

[7] C. Alexandrou, P. de Forcrand, and B. Lucini, Evidence for Diquarks in Lattice QCD, Phys. Rev. Lett. **97**, 222002 (2006).

[8] L. A. Copley, N. Isgur, and G. Karl, Charmed baryons in a quark model with hyperfine interactions, Phys. Rev. D **20**, 768 (1979); **23**, 817(E) (1981).

[9] W. Roberts and M. Pervin, Heavy baryons in a quark model, Int. J. Mod. Phys. A **23**, 2817 (2008).

[10] Y. Yamaguchi, S. Ohkoda, A. Hosaka, T. Hyodo, and S. Yasui, Heavy quark symmetry in multihadron systems, Phys. Rev. D **91**, 034034 (2015).

[11] T. Kawanai and S. Sasaki, Interquark Potential with Finite Quark Mass from Lattice QCD, Phys. Rev. Lett. **107**, 091601 (2011).

[12] S. Takeuchi, Effects of Instantons on P-Wave Multiquark Systems, Phys. Rev. Lett. **73**, 2173 (1994).

[13] E. Hiyama, Y. Kino, and M. Kamimura, Gaussian expansion method for few-body systems, Prog. Part. Nucl. Phys. **51**, 223 (2003).

[14] J.-X. Lu, Y. Zhou, H.-X. Chen, J.-J. Xie, and L.-S. Geng, Dynamically generated $J^P = 1/2^-(3/2^-)$ singly charmed and bottom heavy baryons, Phys. Rev. D **92**, 014036 (2015).

[15] C. Garcia-Recio, C. Hidalgo-Duque, J. Nieves, L. L. Salcedo, and L. Tolos, Compositeness of the strange, charm, and beauty odd parity Λ states, Phys. Rev. D **92**, 034011 (2015).

[16] Y. Namekawa *et al.* (PACS-CS Collaboration), Charmed baryons at the physical point in $2+1$ flavor lattice QCD, Phys. Rev. D **87**, 094512 (2013).

[17] H. Na and S. Gottlieb, Heavy baryon mass spectrum from lattice QCD with $2+1$ dynamical sea quark flavors, *Proc. Sci.*, LATTICE2008 (2008) 119.

[18] C. Albertus, E. Hernandez, J. Nieves, and J. Verde-Velasco, Static properties and semileptonic decays of doubly heavy baryons in a nonrelativistic quark model, Eur. Phys. J. A **32**, 183 (2007).

[19] J. O. Ojo, R. O. Osoniyi, and A. O. Aboderin (SELEX Collaboration), First observation of doubly charmed baryons, Czech. J. Phys. **53**, B201 (2003).

[20] B. Aubert *et al.* (*BABAR* Collaboration), Search for doubly charmed baryons Ξ_{cc}^+ and Ξ_{cc}^{++} in BABAR, Phys. Rev. D **74**, 011103 (2006).

[21] R. Chistov *et al.* (Belle Collaboration), Observation of New States Decaying into $\Lambda_c^+ K^- \pi^+$ and $\Lambda_c^+ K_S^0 \pi^-$, Phys. Rev. Lett. **97**, 162001 (2006).

[22] S. Ogilvy (LHCb Collaboration), Studies of charmed baryons at LHCb, *Proceedings of the 6th International Workshop on Charm Physics (Charm 2013)* (2013), arXiv:1312.1601.